Research Highlights

- Micromilling produced carbon particles with D50s as low as 140 nm.
- Adsorption capacity decreased as D50 decreased from a few micrometers to 140 nm.
- The adsorption capacity decrease was due to carbon oxidization during micromilling.
- Inhibition of carbon oxidation attenuated the decrease in adsorption capacity.
- Adsorption capacity was negatively correlated with particle oxygen content.

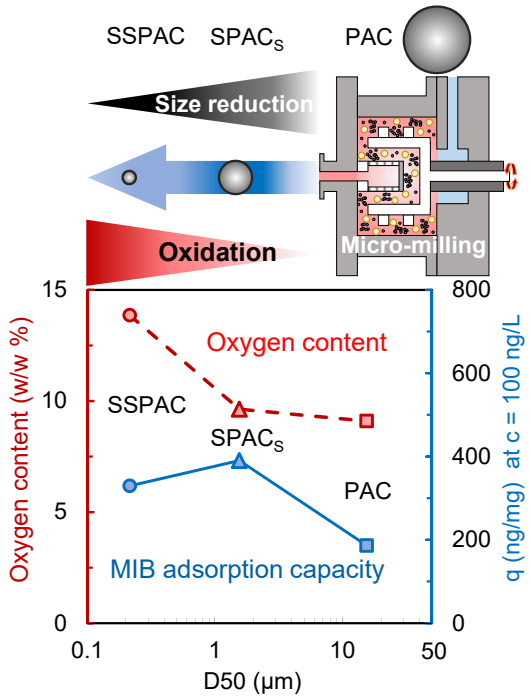
SSPAC
SPACS
PAC
Size reduction
Oxidation
Micro-milling
Oxygen content
SSPAC
SPACS
PAC
MIB adsorption capacity
Oxygen content (w/w %)
q (ng/mg) at c = 100 ng/L
D50 (μm)
0
5
10
15
0
200
400
600
800
0.1
1
10
50

Effects of Decreasing Activated Carbon Particle Diameter from 30 μm to 140 nm on Equilibrium Adsorption Capacity

Long Pan[a], Yuki Nishimura[a], Hideki Takaesu[a], Yoshihiko Matsui[b]*, Taku Matsushita[b], and Nobutaka Shirasaki[b]

[a] Graduate School of Engineering, Hokkaido University, N13W8, Sapporo 060-8628, Japan

[b] Faculty of Engineering, Hokkaido University, N13W8, Sapporo 060-8628, Japan

* Corresponding author. Tel./fax: +81-11-706-7280

E-mail address: matsui@eng.hokudai.ac.jp

Abstract

The capacity of activated carbon particles with median diameters (D50s) of >~1 μm for adsorption of hydrophobic micropollutants such as 2-methylisolborneol (MIB) increases with decreasing particle size because the pollutants are adsorbed mostly on the exterior (shell) of the particles owing to the limited diffusion penetration depth. However, particles with D50s of <1 μm have not been thoroughly investigated. Here, we prepared particles with D50s of ~30 μm to ~140 nm and evaluated their adsorption capacities for MIB and several other environmentally relevant adsorbates. The adsorption capacities for low-molecular-weight adsorbates, including MIB, deceased with decreasing particle size for D50s of less than a few micrometers, whereas adsorption capacities increased with decreasing particle size for larger particles. The oxygen content of the particles increased substantially with decreasing particle size for D50s of less than a few micrometers, and oxygen content was negatively correlated with adsorption capacity. The decrease in adsorption capacity with decreasing particle size for the smaller particles was due to particle oxidation during the micromilling procedure used to decrease D50 to ~140 nm. When oxidation was partially inhibited, the MIB adsorption capacity decrease was attenuated. For high-molecular-weight adsorbates, adsorption capacity increased with decreasing particle size over the entire range of tested particle sizes, even though particle oxygen content increased with decreasing particle size.

Keywords

MIB, micro-grinding, bead mill, oxygen content, oxidation

1. Introduction

Superfine powdered activated carbon (SPAC), which is produced by micromilling of normal powdered activated carbon (PAC), is a new option for efficiently removing natural organic matter, disinfection byproduct precursors, organic micropollutants, and taste and odor compounds from water (Bonvin et al. 2016, Dunn and Knappe 2013, Heijman et al. 2009, Matsui et al. 2007, Matsui et al. 2004, Matsui et al. 2005, Wang et al. 2011). SPAC offers many advantages over PAC, such as higher adsorption capacity (Ando et al. 2010, Ando et al. 2011, Bonvin et al. 2016, Matsui et al. 2010), faster adsorption kinetics (Dudley 2012, Matsui et al. 2009a, Matsui et al. 2011, Wang et al. 2011), and the ability to attenuate the buildup of transmembrane pressure when used before microfiltration (Ellerie et al. 2013, Li 2014, Matsui et al. 2007, Matsui et al. 2009b).

The higher adsorption capacity of SPAC is of both practical and theoretical interest because in previous studies it had been believed that adsorption occurred in the internal pores of activated carbon (AC) particles and that equilibrium adsorption capacity was therefore independent of particle size (Letterman et al. 1974, Najm et al. 1990, Peel and Benedek 1980).

Previous investigations have reported that the change in the AC particle size caused by micro-milling does not result in any substantial change in the internal pore area (Ando et al. 2010, Matsui et al. 2014, Pan et al. 2017). Therefore, the higher adsorption capacity of SPAC is not related to the internal pore area. More recently, the higher adsorption capacity has been explained in terms of the shell adsorption model (SAM), which holds that adsorbates are adsorbed mainly on the exterior (shell) of particles owing to the limited diffusion penetration depth (Ando et al. 2011, Matsui et al. 2011, Matsui et al. 2013, Matsui

et al. 2014). The decrease in particle size upon micromilling increases the exterior surface area, thus enhancing adsorption capacity, as long as the particle radius is larger than the diffusion penetration depth, which depends on the adsorbate and the AC. For example, it has been shown that 2-methylisoborneol (MIB), a taste and odor compound that is a target of water treatment processes, penetrates to a depth of 4–6 μm in some coconut-shell-based and wood-based PACs and that SPACs (particle radius, 0.5–1 μm) produced from the PACs have higher MIB adsorption capacities than the PACs (particle radius, 5–10 μm) (Matsui et al. 2015, Matsui et al. 2014).

The SAM also suggests that if the adsorbate penetration depth is a few micrometers, adsorption capacity may not increase when the AC particle radius is decreased from a few micrometers to less than a micrometer. However, adsorption capacities and characteristics of ACs in this particle size range have not been thoroughly investigated. Micromilling is a new nanotechnology that has enabled production of particles with median diameters (D50s) from the submicrometer range down to hundreds of nanometers, and even smaller (Mende et al. 2003, 2004). This technology has been applied to materials such as corundum (Stenger et al. 2005), aluminum nitride (Jia et al. 2015, Qiu et al. 2006), $Li_4Ti_5O_{12}$ (Han et al. 2012), barium sulfate (Patel et al. 2014), silica (Patel et al. 2015), and crystalline pyrene (Flach et al. 2016). Our research group (Pan et al. 2015, Pan et al. 2017) and others (Amaral et al. 2016, Partlan et al. 2016) have produced AC particles with D50s of 200–250 nm.

Several full-scale SPAC–microfiltration plants are already being used for drinking water production (Kanaya et al. 2015); in these plants, SPAC with D50s of 1–2 μm is produced onsite and added before membrane filtration. The use of smaller particles (e.g., 150-nm diameter) might enhance adsorptive removal efficiency.

In this study, we produced ACs with D50s of 30 μm to 140 nm and evaluated the effects of particle size on their adsorption capacities for various adsorbates.

2. Experimental

2.1 ACs

Five commercially available PACs (Carbons A–E, Table 1) were milled normally (see sec. 2.2.1) to produce SPACs and submicrometer SPACs (SSPACs). The PACs, SPACs, and SSPACs were given unique four-part designations specifying particle size, parent PAC (A–E), production method, and batch number (where applicable). For the first term, PAC designates particles with D50s of 12.0–28.0 μm; $SPAC_L$, D50s of 3.80–8.10 μm; $SPAC_S$, D50s of 0.794–1.80 μm; and SSPAC, D50s of 0.137–0.230 μm. The third term (used only for $SPAC_L$, $SPAC_S$, and SSPAC) indicates the production method: "N" for normal milling, "N_{ET}" for extended-time normal milling, "OI" for oxidation-inhibiting milling, and "R" for rinsing with pure water (see sec. 2.2 and Tables S1 and S2). For example, SSPAC-C-N-2 is the second batch of an SSPAC produced from PAC-C under normal milling conditions.

2.2 SPAC and SSPAC production

$SPAC_L$ was produced with a closed-chamber ball mill (Nikkato, Osaka, Japan) with 5- and 10-mm-diameter balls. $SPAC_S$ and SSPAC were produced with a bead mill with a re-circulation system (LMZ015, Ashizawa Finetech, Chiba, Japan) with (0.1- or 0.3-mm-diameter ZrO_2 beads. The next two sections describe the milling procedures.

2.2.1 Normal milling

As-received PACs (designated as, e.g., PAC-A) were slurried in pure water (Milli-Q Advantage, Millipore, Bedford, MA, USA) at a concentration of ~15% (w/w) and then milled in the ball mill at <45 rpm for 4–5 h to afford particles with D50s of 3.03–3.90 μm (designated as, e.g., $SPAC_L$-A-N). The slurry was collected from the chamber of the ball mill with pure water and then diluted to ~1% (w/w).

The diluted AC slurry (400 mL) was then milled with the bead mill with 0.3-mm-diameter beads at a rotational speed of 2590 rpm in recirculation mode for 20–30 min to afford particles with D50s of <1.47 μm but >0.915 μm (designated as, e.g., $SPAC_S$-A-N). AC particles with D50s of 137–198 nm were produced from $SPAC_L$ or $SPAC_S$ using the bead mill with 0.1-mm-diameter beads at 3884 rpm in re-circulation mode for 1.5–2 h. In additional experiments, the milling time was extended to 5–7 h. During milling, the slurry was kept at <28 °C by means of a cooling system.

2.2.2 Oxidation-inhibiting milling

As-received PACs were dried in a vacuum chamber for at least 1 h, and then the chamber was filled with N_2 at atmospheric pressure. The PACs in the N_2-filled chamber were rinsed with pure water three times. The PACs obtained in this way are designated as, e.g., PAC-C-R.

The rinsed PAC slurries were adjusted to a concentration of ~15% (w/w) with pure water, transferred to the ball mill filled with N_2 gas, and milled under the conditions used for normal milling. Because collecting the AC slurries under N_2 after milling was difficult, they were collected in air, but as quickly as possible. The collected slurries were adjusted to a concentration of ~1% (w/w) with pure water. The dissolved oxygen concentration was

then reduced to <1 mg/L by allowing N_2 gas to diffuse into the slurries for >1 h. The slurries obtained in this way are designated as, e.g., $SPAC_L$-C-OI.

$SPAC_S$-OI was produced by bead milling of $SPAC_L$-OI under conditions in which the slurry was purged with N_2 (Fig. 1); otherwise, the milling conditions were the same as those used for normal bead milling. After milling, the slurries were kept under vacuum for >1 h and then placed under N_2 at atmospheric pressure. The slurries obtained in this way are designated as, e.g., $SPAC_S$-C-OI.

SSPAC-OI was produced by bead milling $SPAC_L$-OI (400–500 mL) under N_2 purging, similar to those used to produce $SPAC_S$, for 3–4 h at 2590 rpm with 0.1- or 0.3-mm-diameter beads.

All the AC slurries were stored at 4 °C after vacuum conditioning to remove air from the pores.

2.3 AC characterization

Particle size distributions of all the ACs were measured by laser-light scattering (Microtrac MT3300EXII, Nikkiso, Tokyo, Japan) in transmission mode. Samples of stock slurries were pretreated with a dispersant (Triton X-100, Kanto Chemical, Tokyo, Japan; final concentration, 0.08% w/v) and ultrasonically dispersed (150 W, 19.5 kHz, 4 min for 50 mL AC slurry) before measurement.

SSPAC particles were observed by field emission scanning electron microscopy (JSM-7400F, JEOL, Tokyo, Japan) at an accelerating voltage of 5.0 kV and a working distance of 3.0 mm. The particles were not precoated, because the thickness of the coating layer might have hindered accurate observation. $SPAC_L$, $SPAC_S$, and PAC particles were not

observed microscopically, because images of these particles had already been obtained (Ando et al. 2010) and because the particles sizes were visually confirmed.

The oxygen, hydrogen, nitrogen, and sulfur contents of the ACs were determined by elemental analysis (Vario EL Cube, Elementar Japan, Yokohama, Japan) with thermal conductivity and infrared detection. For this purpose, the AC slurries were dried by a vacuum cooling method to prevent oxidation during drying. Before elemental analysis, the dried samples were placed in small tin capsules and weighed out. The capsules containing sample were stored in an acrylic container under a vacuum. After atmospheric pressure N_2 was introduced to the box, the capsules were promptly transferred to the elemental analyzer. The oxygen content was measured in O mode, and the other elements were measured in CHNS mode. Ash contents were determined by igniting oven-dried AC samples in a muffle furnace at 550 °C. Averages of triplicate measurements are reported for each AC.

2.4 Adsorbates and working solution

MIB was the main target compound in this study. MIB concentrations were determined in two ways. Either the *m/z* 95 peak of MIB was detected with a purge-and-trap concentrator (Aqua PT 5000 J, GL Sciences, Tokyo, Japan) coupled to a gas chromatograph–mass spectrometer (GCMS-QP2010 Plus, Shimadzu, Kyoto, Japan) using geosmin-d_3 (*m/z* 115) as an internal standard. Or the *m/z* 108 peak of MIB was detected by headspace solid-phase microextraction (PAL RSI 85, Agilent Technologies Japan, Ltd., Tokyo, Japan) coupled to a gas chromatograph–mass spectrometer (7820A/5977 E MSD, Agilent) using 2,4,6-trichloroanisole-d_3 (*m/z* 195) as an internal standard.

On the basis of environmental relevancy, molecular size, and hydrophobicity, nine other adsorbates were tested in addition to MIB: geosmin (log Kow, 3.57; 182 Da),

dimethylphosphorothidate-oxon (DMTP-oxon; log Kow, 0.77; 286 Da), benzothiazole (log Kow, 2.09; 135 Da), phenol (log Kow, 1.46; 94 Da), *para*-nitrophenol (log Kow, 1.91; 139 Da), salicylic acid (log Kow, 2.06; 138 Da), poly(styrenesulfonic acid sodium salt) with an average molecular weight (MW) of 210 Da (PSS-210), PSS-1100 (average MW, 1100 Da), and SNOM (Suwannee River natural organic matter, International Humic Substance Society). Note that the log Kow values listed above are from EPI Suite™ database (ver. 4, U.S. Environmental Protection Agency). Geosmin concentrations were determined by a method similar to that used for MIB; *m/z* 112 was attributed to geosmin. DMTP-oxon was quantified by hybrid quadrupole-orbitrap mass spectrometry (Q Exactive, Thermo Fisher Scientific, Waltham, MA, USA) combined with liquid chromatography (UltiMate3000 LC systems, Thermo Fischer Scientific) using mepronil as an internal standard (DMTP-oxon, *m/z* 287; mepronil, *m/z* 270). The other adsorbate concentrations were measured by UV–vis spectrophotometry (UV-1800, Shimadzu, Kyoto, Japan) at 269.5, 252, 296, 317, and 261 nm for phenol, benzothiazole, salicylic acid, *para*-nitrophenol, and PSS-210/PSS-1100, respectively.

Except for PSS-210 and PSS-1100 (Sigma-Aldrich, St. Louis, MO, USA), all chemical reagents were purchased from Wako Pure Chemical Industries (Osaka, Japan). The working solution was organic-free water with the ion composition used in previous research (Table S3) (Matsui et al. 2015, Pan et al. 2016). The working solutions were adjusted to pH 7.0 ± 0.1 with HCl or NaOH as required. The solution pH was maintained constant during adsorption tests probably due to bicarbonate buffer.

2.5 Batch adsorption tests

For each target adsorbate, an aliquot (100 or 110 mL) of working solution containing the adsorbate was transferred to a 110-mL vial; AC was immediately added; and the vial

was manually shaken and then agitated on a mechanical shaker for 1 week or 3 days at 20 °C in the dark. Preliminary experiments confirmed that adsorption equilibrium was reached within 1 week for the MIB–PAC combination (Matsui et al. 2013, Matsui et al. 2012), 3 days for MIB–SPAC/SSPAC, and 1 week for the other 8 adsorbates (for all the ACs). Control tests of blank solutions containing adsorbates but no AC confirmed that changes in adsorbate concentration during long-term mixing were negligible. After shaking, water samples were filtered through a 0.2-μm-pore-size membrane filter (polytetrafluoroethylene, DISMIC-25HP, Toyo Roshi Kaisha, Tokyo, Japan) to remove the AC, and then the adsorbate concentration in the filtrate was measured. Complete removal of SSPAC required two filtrations. Preliminary tests confirmed that MIB did not adsorb on the filter and that SSPAC was completely removed by the filtration. Solid-phase concentrations of adsorbates were calculated from mass balances.

3. Results and discussion

3.1 SPAC and SSPAC production by normal micromilling

SSPACs with D50s of 137–198 nm were produced by the milling methods described in sec. 2.1, and SSPAC production with good reproducibility was verified both from the particle size distribution (Fig. S1) and by scanning electron microscopy (Fig. 2). The characteristics of the normally milled ACs are listed in Table S1.

3.2 Effects of particle size on MIB adsorption capacity

Equilibrium MIB adsorption isotherms were determined for Carbons A with D50s of 12.0–0.198 μm (Fig. S2). The MIB adsorption capacity of each AC was quantified in terms of the solid-phase concentrations (designated as q) in equilibrium with liquid-phase concentrations of 50 and 100 ng/L, after fitting of the isotherm data to the Freundlich model.

The effects of particle size on MIB adsorption capacity are depicted in Fig. 3a. Reduction of D50 from 12.0 μm (PAC-A) to 1.47 μm (SPAC$_S$-A-N) doubled the adsorption capacity, but the MIB adsorption capacity did not increase when D50 was decreased further: the MIB adsorption capacity of SSPAC-A-N (D50: 198 nm) was ~85% of that of SPAC$_S$-A-N.

A decrease in adsorption capacity in going from SPAC$_S$ to SSPAC was also observed for the other ACs. For example, the adsorption capacity of SSPAC-B-N was ~90% of that of SPAC$_S$-B-N, the adsorption capacity of SSPAC-C-N was 51–93% of that of SPAC$_S$-C-N, and the adsorption capacity of SSPAC-D-N was ~90% of that of SPAC$_S$-D-N (Fig. 3b–d, respectively). The adsorption capacity of SSPAC-D-N$_{ET}$, which was produced by milling for extended time, was 65–75% of that of SPAC$_S$-D-N. In the case of Carbons E, the adsorption capacity started to decrease with particle size when D50 was <3.90 μm; the adsorption capacity of SSPAC-E-N was ~74% of that of SPAC$_L$-E-N (Fig. 3e). A similar trend was reported in a study of atrazine removal with microfiltration membrane precoated with SPAC (Amaral et al. 2016). In that study, adsorption capacity decreased as D50 was reduced from ~300 to ~200 nm for one of the three studied ACs and as D50 was reduced from ~600 to ~500 nm for another AC, although the authors of the paper did not comment on the trend.

According to the SAM, adsorbent particle size affects MIB adsorption capacity when the adsorbent radius is substantially larger than the adsorbate penetration depth (Matsui et al. 2013, Matsui et al. 2014). Under these circumstances, the increase in the external surface area of the adsorbent particles with decreasing particle size results in increased adsorption capacity. Therefore, the higher adsorption capacity of PAC-A (12.0 μm) relative to that of SPAC$_S$-A-N (1.47 μm) was likely due to this mechanism. That the adsorption capacity did not increase with decreasing particle size for D50s of <1.47 μm (i.e., from SPAC$_S$-A-N to SSPAC-A-N) suggests that the particle radii of both of these ACs were smaller than the

MIB penetration depth and that all of the internal pores of the particles were utilized for MIB adsorption. Once the internal pores are completely utilized, adsorption capacity is independent of particle size. The change in the AC particle size caused by micromilling would not result in any substantial change in the internal pore structure (Ando et al. 2010, Matsui et al. 2014, Pan et al. 2017). Moreover, any structural changes in internal pores could not explain the phenomena that MIB adsorption capacity decreased while PSS-1100 adsorption capacity increased, as described in the section 3.6. Under these circumstances, pore surface chemistry strongly would affect adsorption capacity (Li et al. 2002, Matsui et al. 2015, Quinlivan et al. 2005).

3.3 Oxygen content of AC

Oxygen-containing complexes on the AC surface alter surface hydrophobicity and affect the adsorption capacity for organic compounds, including MIB (Moreno-Castilla 2004, Pendleton et al. 1997, Song et al. 2010). The number of oxygen-containing complexes is reflected by the AC oxygen content (% [w/w]), which is thus highly correlated with MIB adsorption capacity (Li et al. 2002, Matsui et al. 2015).

The oxygen content of Carbons A increased with decreasing particle size (Fig. 4a), and the increase was particularly large when D50 dropped to <1 μm. The external surface of AC particles is usually more oxidized than the interior because oxygen diffuses very slowly in the abundant, narrow internal pores (Boehm 2002). Micromilling in the bead mill, which was used to produce particles with D50s of <1 μm, brought the particle interior into contact with oxygen in the water, possibly hastening oxidation. That the drop in MIB adsorption capacity was coincident with a substantial increase in oxygen content (Figs. 3 and 4) suggests that the drop in MIB adsorption capacity was due to carbon oxidation.

Wood-based Carbons A–C (i.e., PAC-A, PAC-B, and PAC-C) were produced by the same manufacturer, and were marketed under the same specification and brand name. However, they were produced in different batches, and were received in our laboratory at different times. In addition, the times from receipt to experimental use (stock periods) differed, decreasing in the order PAC-A (~7 years) > PAC-B (~1 year) > PAC-C (<6 months). This order is consistent with the order of decreasing oxygen content: PAC-A (9.1%) > PAC-B (7.2%) > PAC-C (2.0%) (Fig. 4a–c). This finding is in line with a report that AC is oxidized very slowly in air (Billinge et al. 1984, Boehm 2002). For these three PACs, the order of decreasing MIB adsorption capacity was opposite the order of decreasing oxygen content: that is, adsorption capacity decreased with carbon age in the order PAC-C > PAC-B > PAC-A (Fig. S2). Although characteristics other than oxygen content might also be related to the adsorption capacity difference between the three carbons, these data is consistent with the idea that carbon oxidation decreased MIB adsorption capacity (Considine et al. 2001).

For Carbons A–C, the sources of which had different oxygen contents, oxygen content increased as the particle size was decreased by micromilling with the bead mill (Fig. 4a–c). The same was true of Carbon D, a wood-based AC produced by a different manufacturer, and Carbon E, a coal-based AC produced by a third manufacturer (Fig. 4d,e). The oxygen content increased further when the milling time was extended from 1.5–2 to 5–7 h (compare SSPAC-D-N and SSPAC-D-N_{ET} in Fig. 4d). Because the external surface of AC particles is believed to be more oxidized than the interior (Boehm 2002, Partlan et al. 2016), overall particle oxidation would have increased as particle size was decreased by micromilling. That oxygen content increased with decreasing particle size for all five kinds of ACs used in this study is consistent with this understanding.

3.4 Controlling oxidation during SPAC and SSPAC production

The increase in oxygen content as milling progressed suggests that milling introduced oxygen-containing functional groups, which would increase the carbon hydrophilicity and thus decrease MIB adsorption capacity. Therefore, if oxidation during milling could be inhibited, the adsorption capacity decrease could be attenuated. We investigated various methods for producing less-oxidized SSPAC with D50s of <230 nm (Table S2, Fig. S1). The oxygen contents of Carbons C and D are presented in Fig. 5 (Fig. S3).

Oxidation-inhibiting milling (sec. 2.2.2) inhibited oxidation as D50 was reduced from 2.65-8.11 μm to 174–230 nm. Specifically, oxidation-inhibiting milling to produce SSPAC-C-OI increased oxygen content by only 2.2 ± 0.5% (w/w) (Fig. 5c), whereas normal milling to produce SSPAC-C-N increased oxygen content by 3.4 ± 1.2% (Fig. 4c). The oxygen content increase in going from $SPAC_L$-D to SSPAC-D by oxidation-inhibiting milling was 2.0 ± 0.2% (Fig. 5d), which was approximately half the increase due to normal milling (3.8 ± 0.1%; Fig. 4d).

We also measured the hydrogen, nitrogen, sulfur, and ash contents of ACs produced by normal milling and oxidation-inhibiting milling (Fig. S4). Like oxygen content, hydrogen content increased with decreasing particle size. When the particles were milled, the ratio (increase in oxygen content, in moles)/(increase in hydrogen content, in moles) ranged from 2/3 to 3/2. This result suggests that hydroxyl and/or carboxyl groups formed on the carbon surface, an additional indication that milling increased carbon hydrophilicity. The ash contents in PAC-B-R, $SPAC_S$-B-OI, SSPAC-B-OI, and SSPAC-B-N were somewhat lower than those in PAC-B and $SPAC_S$-B-N. This result may have been due to the effect of rinsing and dilution of the AC slurry with pure water; rinsing and dilution would have washed out inorganic materials, including metals. However, this small change

in ash content did not affect MIB adsorption capacity: the MIB adsorption isotherm of PAC-C-R did not differ substantially from that of PAC-C (Fig. S5).

3.5 Correlation between oxygen content and MIB adsorption capacity

We have suggested that the low MIB adsorption capacities of the SSPACs produced by normal milling resulted from carbon oxidation. In a final test, SSPACs with low oxygen content (SSPAC-C-OI) and with high oxygen content (SSPAC-C-N) were produced from the same PAC, and their MIB adsorption capacities were determined. SSPAC-C-OI exhibited higher adsorption capacity than SSPAC-C-N (Figs. S2 and S6). Moreover, there were strong negative correlations between oxygen content and MIB adsorption capacity (Fig. 6). These results clearly indicate that the low MIB adsorption capacity of normally milled SSPAC produced relative to that of SPACs was due to increased oxygen content, which increased carbon hydrophilicity.

The plots in Fig. 6 include data for AC particles with D50s from 137 nm to 1.64 μm (i.e., all the SPACss and SSPACs). The correlation shown in the figure clearly means that adsorption capacity was unrelated to particle size in this range, suggesting that the entire particle, including internal pores, was accessible to MIB molecules, as suggested by the SAM (sec. 3.1). Oxygen content is a good indicator of MIB adsorption capacity of particles with D50s of < ~1 μm (SPACs and SSPAC). This agrees with a previous finding that SPAC hydrophilicity, as indicated by oxygen content, is the main determinant of adsorption capacity for hydrophobic compounds such as geosmin (Matsui et al., 2015).

The oxygen content of SSPAC-OI was lower than that of SSPAC-N but was still higher than that of the SPACs from which SSPACs were produced. That is, oxidation was not completely prevented by oxidation-inhibiting milling. The highest adsorption capacity was

attained with SPACs having a D50 of ~1 μm. The energy required to reduce D50 to < ~1 μm would not offer any increase in adsorption capacity. Therefore, SPAC with a D50 of a few micrometers (~1.5 μm for Carbons A–D, ~4.0 μm for Carbon E) is a more reasonable choice for MIB removal from the viewpoint of high MIB adsorption capacity and reasonable energy consumption.

3.6 Effect of particle size on adsorption of other adsorbates

We observed that adsorption capacity for MIB, a hydrophobic low-MW compound (log Kow, 3.31; 168 Da), increased in going from PAC to SPAC and decreased in going from SPAC to SSPAC. To determine whether this trend held for other adsorbates, we conducted adsorption equilibrium tests on several environmentally relevant compounds with various hydrophobicities and MWs. The adsorption capacities for these compounds were quantified in terms of the solid-phase concentrations (q) in equilibrium with two liquid-phase concentrations in the experimentally observed range (Fig. S6). Then we evaluated the relationship between adsorption capacity and particle size (Fig. S8).

Going from SPACs-A-N (1.47 μm) to SSPAC-A-N (0.20 μm) did not decrease adsorption capacity for PSS-1100 and SNOM, which have high MWs (>1000 Da, Fig. S8); in fact, adsorption capacity consistently increased with decreasing particle size. This result is consistent with previous findings indicating that adsorption capacity for high-MW compounds increases with decreasing AC particle size (Ando et al. 2010, Ando et al. 2011). For high-MW compounds, the penetration depth was smaller than the radii of adsorbents such as PAC and SPAC (Ando et al. 2010); therefore the interior of those adsorbents were inaccessible to those adsorbates, and adsorption occurred only at the external particle surface. In these circumstances, adsorption capacity increases with decreasing adsorbent particle size.

For the other 7 compounds, all of which had MWs of <300 Da, adsorption capacity decreased when D50 was decreased to < ~1 μm, as was the case for MIB. For all the adsorbates, the adsorption capacities of SSPAC-A-N (0.20 μm) were lower than those of SPACs-A-N (1.47 μm) (Figs. 7 and S8). The magnitude of the adsorption capacity decrease depended on the adsorbate, but we were unable to identify the adsorbate property that explained the magnitude of the decrease. For example, the magnitude of the decrease was not correlated to adsorbate log Kow (R^2 < 0.02, Figs. 7 and S9a). The adsorption capacity of SSPAC-A-N for geosmin (log Kow, 3.57), which is at least as hydrophobic as MIB (log Kow, 3.31), was 30% lower than that of SPACs-A-N. The adsorption capacity of SSPAC-A-N for DMTP-oxon (log Kow, 0.77), which is hydrophilic, was also 30% lower than that of SPACs-A-N. For Carbons B (i.e., SPACs-B-N and SSPAC-B-N), the magnitude of the adsorption capacity decrease was not correlated with adsorbate log Kow (Fig. S9b,c). The lower adsorption capacity of SSPAC relative to that of SPACs was due to the higher hydrophilicity of SSPAC, as indicated by the higher oxygen content (sec. 3.5). The differences in the magnitude of the adsorption capacity decease in going from SPACs to SSPAC for the eight compounds (MIB plus the seven adsorbates other than PSS-1100 and SNOM) indicate that the adsorption capacities for these compounds had different sensitivities to carbon hydrophilicity (oxygen content).

Different sensitivities to carbon hydrophilicity have been reported in other studies, although these studies did not involve SPAC or SSPAC. For example, a study comparing the adsorption capacities of AC for a hydrophobic compound, trichloroethene (log Kow, 2.42; 131 Da), and a hydrophilic compound, methyl *tert*-butyl ether (log Kow, 0.94; 88 Da), indicated that the decrease in adsorption capacity associated with increased carbon hydrophilicity was more pronounced for the hydrophilic compound (i.e., the adsorbate with the lower log Kow) (Li et al. 2002). However, a study involving several fatty acids,

including propanoic acid (log Kow, 0.33; 74.1 Da), valeric acid (log Kow, 1.39; 102 Da), enanthic acid (log Kow, 2.42; 130 Da), and pelargonic acid (log Kow, 3.42; 158 Da), revealed that the decrease in adsorption capacity associated with increased carbon hydrophilicity was not necessarily greater for hydrophobic adsorbates with high log Kow values than for hydrophilic adsorbates with low log Kow values (Kaneko et al. 1989). Water likely adsorbs as clusters around the hydrophilic sites on the carbon surface (Pendleton et al. 1997). As the number of hydrophilic sites increases, water clusters tend to extend over hydrophobic sites, which prevents hydrophobic adsorbates, such as MIB, from accessing the hydrophobic sites on the carbon surface. Increased formation of water clusters on hydrophilic sites also reduces the energy of interaction between hydrophilic adsorbates, such as DMTP-oxon, and the carbon surface (Kaneko et al. 1989, Li et al. 2002). Although adsorption capacity for both hydrophobic and hydrophilic adsorbates decreases with decreasing carbon hydrophobicity, the mechanisms of the decreases for the two types of adsorbates are likely to differ, which in turn would lead to differences in the sensitivity of adsorption capacity to carbon hydrophobicity.

4. Conclusions

(1) Micromilling produced AC particles with D50s as low as 137 nm.

(2) MIB adsorption capacity decreased with decreasing particle size for ACs with D50s of less than a few micrometers. This decrease in adsorption capacity was due to carbon oxidization during micromilling.

(3) Partial inhibition of carbon oxidation during micromilling attenuated the decrease in MIB adsorption capacity.

(4) For attaining high MIB adsorption capacity without unnecessary consumption of energy for micromilling, SPAC with a D50 of 1–4 μm is a reasonable choice.

(5) The adsorption capacity decrease with decreasing AC particle size for particles with D50s of less than a few micrometers was observed for all eight low-MW adsorbates. The magnitude of the decrease depended on the adsorbates, but the relationship could not be explained simply by differences in adsorbate hydrophilicity.

(6) For SNOM and PSS-1100, adsorption capacity increased with decreasing adsorbent particle size (i.e., in going from PAC to SSPAC).

(7) AC underwent oxidation during long-term storage, and the resulting increase in oxygen content could be associated with decreases in adsorption capacity for compounds such as MIB.

Acknowledgments

This study was supported by a Grant-in-Aid for Scientific Research S (16H06362) from the Japan Society for the Promotion of Science and was partly supported by a Health and Labor Sciences Research Grant (H28-Kenki-Ippan-005) from the Ministry of Health, Labour, and Welfare, Japan. We acknowledge the financial support in the form of a scholarship (201306460006) from the China Scholarship Council (CSC) to Long Pan for his doctoral research.

Appendix. Supplementary Information

Table S1-S3 and Figures S1–S9 are available in the online version at ######.

444

445

References

Amaral, P., Partlan, E., Li, M., Lapolli, F., Mefford, O.T., Karanfil, T. and Ladner, D.A. (2016) Superfine powdered activated carbon (S-PAC) coatings on microfiltration membranes: Effects of milling time on contaminant removal and flux. Water Research 100, 429-438.

Ando, N., Matsui, Y., Kurotobi, R., Nakano, Y., Matsushita, T. and Ohno, K. (2010) Comparison of natural organic matter adsorption capacities of super-powdered activated carbon and powdered activated Carbon. Water Research 44(14), 4127-4136.

Ando, N., Matsui, Y., Matsushita, T. and Ohno, K. (2011) Direct observation of solid-phase adsorbate concentration profile in powdered activated carbon particle to elucidate mechanism of high adsorption capacity on super-powdered activated carbon. Water Research 45(2), 761-767.

Billinge, B.H.M., Docherty, J.B. and Bevan, M.J. (1984) The desorption of chemisorbed oxygen from activated carbons and its relationship to ageing and methyl iodide retention efficiency. Carbon 22(1), 83-89.

Boehm, H.P. (2002) Surface oxides on carbon and their analysis: a critical assessment. Carbon 40(2), 145-149.

Bonvin, F., Jost, L., Randin, L., Bonvin, E. and Kohn, T. (2016) Super-fine powdered activated carbon (SPAC) for efficient removal of micropollutants from wastewater treatment plant effluent. Water Research 90, 90-99.

Considine, R., Denoyel, R., Pendleton, P., Schumann, R. and Wong, S.-H. (2001) The influence of surface chemistry on activated carbon adsorption of 2-methylisoborneol from aqueous solution. Colloids and Surfaces A: Physicochemical and Engineering Aspects 179(2–3), 271-280.

Dudley, L.-A. (2012) Removal of Perfluorinated Compounds by Powdered Activated Carbon, Superfine Powder Activated Carbon, and Anion Exchange Resin.

Dunn, S.E. and Knappe, D.R. (2013) DBP Precursor and Micropollutant Removal by Powdered Activated Carbon [Project# 4294].

Ellerie, J.R., Apul, O.G., Karanfil, T. and Ladner, D.A. (2013) Comparing graphene, carbon nanotubes, and superfine powdered activated carbon as adsorptive coating materials for microfiltration membranes. Journal of Hazardous materials, 261, 91-98.

Flach, F., Konnerth, C., Peppersack, C., Schmidt, J., Damm, C., Breitung-Faes, S., Peukert, W. and Kwade, A. (2016) Impact of formulation and operating parameters on

particle size and grinding media wear in wet media milling of organic compounds – A case study for pyrene. Advanced Powder Technology 27(6), 2507-2519.

Han, S.-W., Shin, J.-W. and Yoon, D.-H. (2012) Synthesis of pure nano-sized Li4Ti5O12 powder via solid-state reaction using very fine grinding media. Ceramics International 38(8), 6963-6968.

Heijman, S.G.J., Hamad, J.Z., Kennedy, M.D., Schippers, J. and Amy, G. (2009) Submicron powdered activated carbon used as a pre-coat in ceramic micro-filtration. Desalination and Water Treatment 9(1-3), 86-91.

Jia, L., Kondoh, K., Imai, H., Onishi, M., Chen, B. and Li, S.-f. (2015) Nano-scale AlN powders and AlN/Al composites by full and partial direct nitridation of aluminum in solid-state. Journal of Alloys and Compounds 629, 184-187.

Kanaya, S., Kawase, Y., Mima, S., Sugiura, K., Murase, K. and Yonekawa, H. (2015) Drinking Water Treatment Using Superfine PAC (SPAC): Design and Successful Operation History in Full-Scale Plant, Salt Lake City, Utah, USA.

Kaneko, Y., Abe, M. and Ogino, K. (1989) Adsorption characteristics of organic compounds dissolved in water on surface-improved activated carbon fibres. Colloids and Surfaces 37, 211-222.

Letterman, R.D., Quon, J. and Gemmell, R.S. (1974) Film transport coefficient in agitated suspensions of activated carbon. Journal (Water Pollution Control Federation), 2536-2546.

Li, L., Quinlivan, P.A. and Knappe, D.R.U. (2002) Effects of activated carbon surface chemistry and pore structure on the adsorption of organic contaminants from aqueous solution. Carbon 40(12), 2085-2100.

Li, M. (2014) Effects of Natural Organic Matter on Contaminant Removal by Superfine Powdered Activated Carbon Coupled with Microfiltration Membranes. Thesis of Clemson University.

Matsui, Y., Aizawa, T., Kanda, F., Nigorikawa, N., Mima, S. and Kawase, Y. (2007) Adsorptive removal of geosmin by ceramic membrane filtration with super-powdered activated carbon. Journal of Water Supply: Research & Technology-AQUA 56.

Matsui, Y., Ando, N., Sasaki, H., Matsushita, T. and Ohno, K. (2009a) Branched pore kinetic model analysis of geosmin adsorption on super-powdered activated carbon. Water Research 43(12), 3095-3103.

509 Matsui, Y., Ando, N., Yoshida, T., Kurotobi, R., Matsushita, T. and Ohno, K. (2011)
510 Modeling high adsorption capacity and kinetics of organic macromolecules on super-
511 powdered activated carbon. Water Research 45(4), 1720-1728.

512 Matsui, Y., Hasegawa, H., Ohno, K., Matsushita, T., Mima, S., Kawase, Y. and Aizawa, T.
513 (2009b) Effects of super-powdered activated carbon pretreatment on coagulation and
514 trans-membrane pressure buildup during microfiltration. Water Research 43(20), 5160-
515 5170.

516 Matsui, Y., Murase, R., Sanogawa, T., Aoki, N., Mima, S., Inoue, T. and Matsushita, T.
517 (2004) Micro-ground powdered activated carbon for effective removal of natural organic
518 matter during water treatment. Water Science & Technology: Water Supply 4(4).

519 Matsui, Y., Murase, R., Sanogawa, T., Aoki, N., Mima, S., Inoue, T. and Matsushita, T.
520 (2005) <Rapid adsorption pretreatment with submicrometre powdered activated carbon
521 particles before microfiltration.pdf>. Water Science & Technology 51(6-7), 7.

522 Matsui, Y., Nakano, Y., Hiroshi, H., Ando, N., Matsushita, T. and Ohno, K. (2010) Geosmin
523 and 2-methylisoborneol adsorption on super-powdered activated carbon in the presence
524 of natural organic matter. Water Science & Technology 62(11).

525 Matsui, Y., Nakao, S., Sakamoto, A., Taniguchi, T., Pan, L., Matsushita, T. and Shirasaki,
526 N. (2015) Adsorption capacities of activated carbons for geosmin and 2-methylisoborneol
527 vary with activated carbon particle size: Effects of adsorbent and adsorbate characteristics.
528 Water Research 85, 95-102.

529 Matsui, Y., Nakao, S., Taniguchi, T. and Matsushita, T. (2013) Geosmin and 2-
530 methylisoborneol removal using superfine powdered activated carbon: Shell adsorption
531 and branched-pore kinetic model analysis and optimal particle size. Water Research 47(8),
532 2873-2880.

533 Matsui, Y., Sakamoto, A., Nakao, S., Taniguchi, T., Matsushita, T., Shirasaki, N.,
534 Sakamoto, N. and Yurimoto, H. (2014) Isotope Microscopy Visualization of the Adsorption
535 Profile of 2-Methylisoborneol and Geosmin in Powdered Activated Carbon. Environmental
536 Science & Technology 48(18), 10897-10903.

537 Matsui, Y., Yoshida, T., Nakao, S., Knappe, D.R.U. and Matsushita, T. (2012)
538 Characteristics of competitive adsorption between 2-methylisoborneol and natural organic
539 matter on superfine and conventionally sized powdered activated carbons. Water
540 Research 46(15), 4741-4749.

Mende, S., Stenger, F., Peukert, W. and Schwedes, J. (2003) Mechanical production and stabilization of submicron particles in stirred media mills. Powder Technology 132(1), 64-73.

Mende, S., Stenger, F., Peukert, W. and Schwedes, J. (2004) Production of sub-micron particles by wet comminution in stirred media mills. Journal of Materials Science 39(16), 5223-5226.

Moreno-Castilla, C. (2004) Adsorption of organic molecules from aqueous solutions on carbon materials. Carbon 42(1), 83-94.

Najm, I.N., Snoeyink, V.L., Suidan, M.T., Lee, C.H. and Richard, Y. (1990) Effect of Particle Size and Background Natural Organics on the Adsorption Efficiency of PAC. Journal (American Water Works Association) 82(1), 65-72.

Pan, L., Matsui, Y., Matsushita, T. and Shirasaki, N. (2015) Effect of activated carbon particle size on equilibrium adsorption capacity in the range of 200 nm to 2 mm. The 6th IWA-ASPIRE Conference, Beijing, China. 20-24, September, 2017.

Pan, L., Matsui, Y., Matsushita, T. and Shirasaki, N. (2016) Superiority of wet-milled over dry-milled superfine powdered activated carbon for adsorptive 2-methylisoborneol removal. Water Research 102, 516-523.

Pan, L., Takagi, Y., Matsui, Y., Matsushita, T. and Shirasaki, N. (2017) Micro-milling of spent granular activated carbon for its possible reuse as an adsorbent: Remaining capacity and characteristics. Water Research 114, 50-58.

Partlan, E., Davis, K., Ren, Y., Apul, O.G., Mefford, O.T., Karanfil, T. and Ladner, D.A. (2016) Effect of bead milling on chemical and physical characteristics of activated carbons pulverized to superfine sizes. Water Research 89, 161-170.

Patel, C.M., Chakraborty, M. and Murthy, Z.V.P. (2014) Study on the stability and microstructural properties of barium sulfate nanoparticles produced by nanomilling. Advanced Powder Technology 25(1), 226-235.

Patel, C.M., Chakraborty, M. and Murthy, Z.V.P. (2015) Influence of pH on the Stability of Alumina and Silica Nanosuspension Produced by Wet Grinding. Particulate Science and Technology 33(3), 240-245.

Peel, R.G. and Benedek, A. (1980) Attainment of equilibrium in activated carbon isotherm studies. Environmental Science & Technology 14(1), 66-71.

572 Pendleton, P., Wong, S.H., Schumann, R., Levay, G., Denoyel, R. and Rouquero, J. (1997)
573 Properties of activated carbon controlling 2-Methylisoborneol adsorption. Carbon 35(8),
574 1141-1149.

575 Qiu, J.-Y., Hotta, Y., Watari, K., Mitsuishi, K. and Yamazaki, M. (2006) Low-temperature
576 sintering behavior of the nano-sized AlN powder achieved by super-fine grinding mill with
577 Y2O3 and CaO additives. Journal of the European Ceramic Society 26(4–5), 385-390.

578 Quinlivan, P.A., Li, L. and Knappe, D.R.U. (2005) Effects of activated carbon
579 characteristics on the simultaneous adsorption of aqueous organic micropollutants and
580 natural organic matter. Water Research 39(8), 1663-1673.

581 Song, X., Liu, H., Cheng, L. and Qu, Y. (2010) Surface modification of coconut-based
582 activated carbon by liquid-phase oxidation and its effects on lead ion adsorption.
583 Desalination 255(1), 78-83.

584 Stenger, F., Mende, S., Schwedes, J. and Peukert, W. (2005) Nanomilling in stirred media
585 mills. Chemical Engineering Science 60(16), 4557-4565.

586 Wang, Y., Rao, G.Y. and Hu, J.Y. (2011) Adsorption of EDCs/PPCPs from drinking water
587 by submicron-sized powdered activated carbon. Water Science and Technology: Water
588 Supply 11(6), 711-718.

589

Table 1 – Commercial PACs used in this study.

Designation	Series	Production year	Raw material	Brand name	Manufacture specifications				Manufacture
					Phenol number	Iodine number (mg/g)	Methylene blue number (mL/g)	ABS number	
PAC-A	Carbon-A	2008	wood	Taiko W	< 25	> 900	> 150	< 50	Futamura Chemical Co., Tokyo, Japan
PAC-B	Carbon-B	2015							
PAC-C	Carbon-C	2016							
PAC-D	Carbon-D	2016	wood	Shirasagi	< 25	> 900	> 150	< 50	Osaka Chemical Co., Osaka, Japan
PAC-E	Carbon-E	2016	coal	6MD	< 25	> 900	> 150	< 50	Calgon Carbon Japan KK

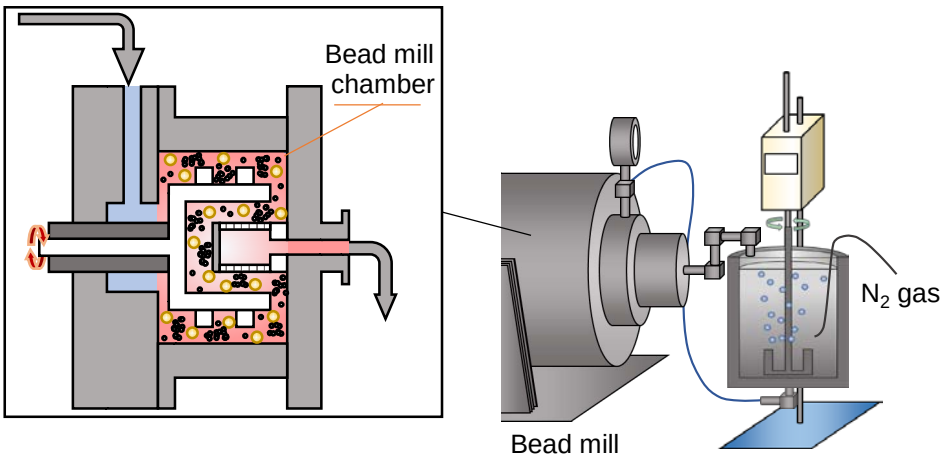

Fig. 1 – Schematic diagram of apparatus for bead milling under N_2.

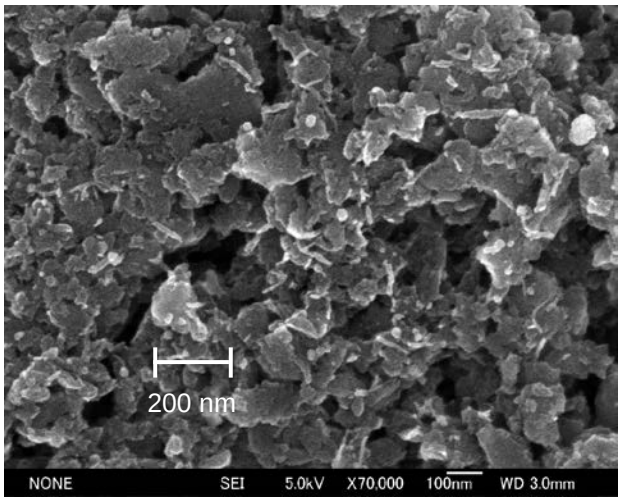

Fig. 2 – Scanning electron micrograph of SSPAC-B-N.

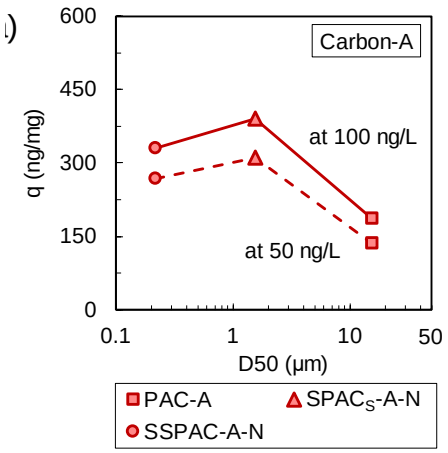
Carbon-A
at 100 ng/L
at 50 ng/L
q (ng/mg)
D50 (μm)
PAC-A
SPAC$_S$-A-N
SSPAC-A-N

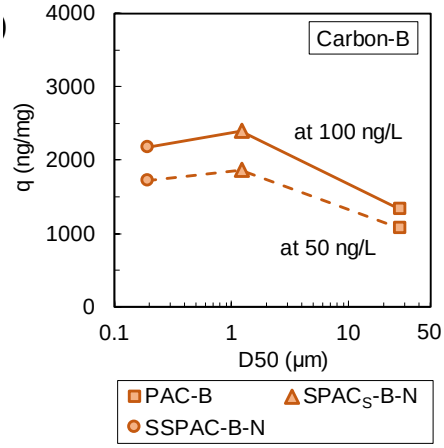
Carbon-B
at 100 ng/L
at 50 ng/L
q (ng/mg)
D50 (μm)
PAC-B
SPAC$_S$-B-N
SSPAC-B-N

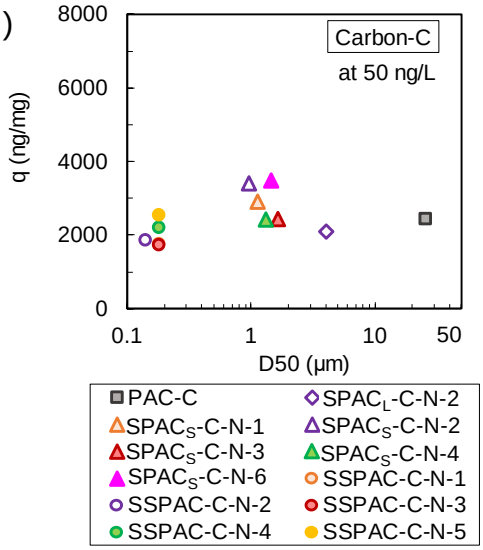
Carbon-C
at 50 ng/L
q (ng/mg)
D50 (μm)
PAC-C
SPAC$_L$-C-N-2
SPAC$_S$-C-N-1
SPAC$_S$-C-N-2
SPAC$_S$-C-N-3
SPAC$_S$-C-N-4
SPAC$_S$-C-N-6
SSPAC-C-N-1
SSPAC-C-N-2
SSPAC-C-N-3
SSPAC-C-N-4
SSPAC-C-N-5

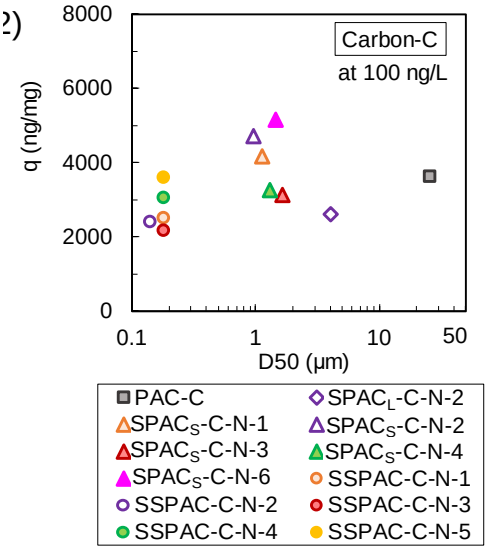
Carbon-C
at 100 ng/L
q (ng/mg)
D50 (μm)
PAC-C
SPAC$_L$-C-N-2
SPAC$_S$-C-N-1
SPAC$_S$-C-N-2
SPAC$_S$-C-N-3
SPAC$_S$-C-N-4
SPAC$_S$-C-N-6
SSPAC-C-N-1
SSPAC-C-N-2
SSPAC-C-N-3
SSPAC-C-N-4
SSPAC-C-N-5

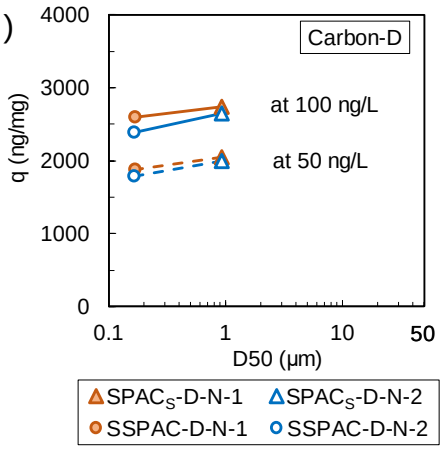
Carbon-D
at 100 ng/L
at 50 ng/L
q (ng/mg)
D50 (μm)
SPAC$_S$-D-N-1
SPAC$_S$-D-N-2
SSPAC-D-N-1
SSPAC-D-N-2

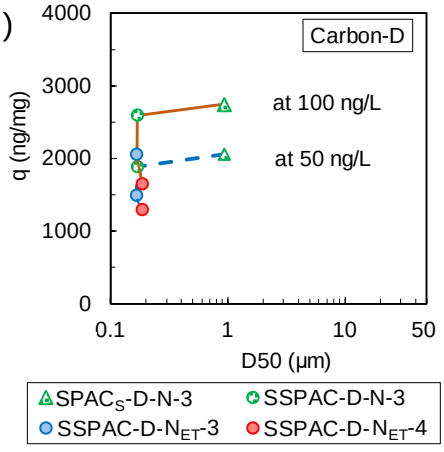
Carbon-D
at 100 ng/L
at 50 ng/L
q (ng/mg)
D50 (μm)
SPAC$_S$-D-N-3
SSPAC-D-N-3
SSPAC-D-N$_{ET}$-3
SSPAC-D-N$_{ET}$-4

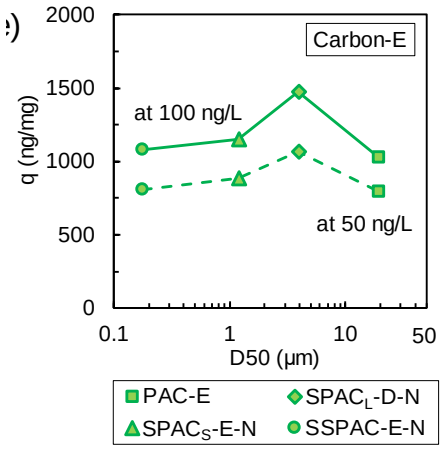

Fig. 3 – Plots of equilibrium MIB adsorption capacity versus AC particle size. Squares indicate PAC, diamonds indicate $SPAC_L$, triangles indicate $SPAC_S$, and circles indicate SSPAC. The adsorption capacities are given as solid-phase concentrations (q) at the equilibrium liquid-phase concentrations of 50 or 100 ng/L.

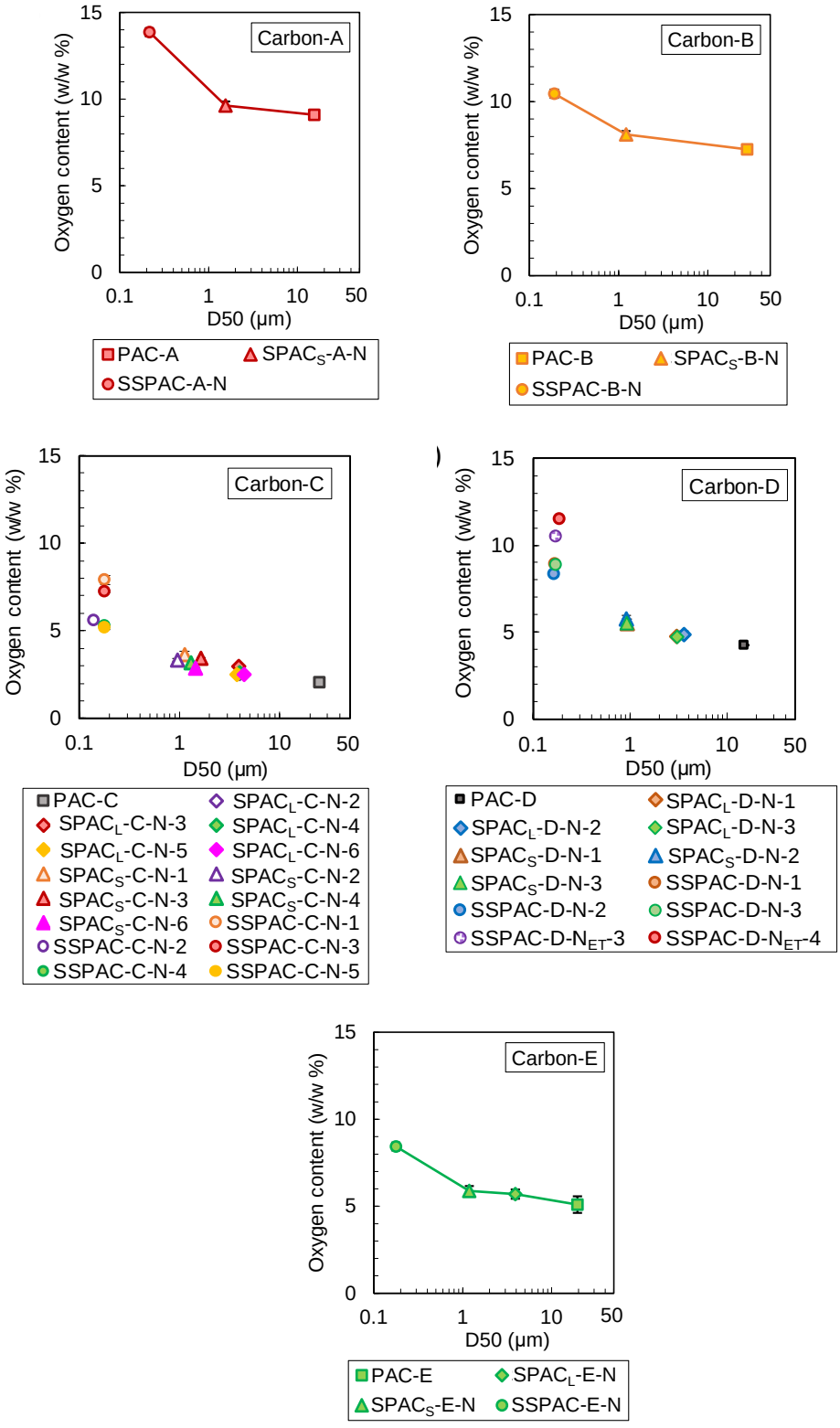

Fig. 4 – Plots of oxygen contents of Carbons A–E produced by normal milling versus AC particle size. Squares indicate PAC, diamonds indicate SPAC$_L$, triangles indicate SPAC$_S$, and circles indicate SSPAC. Error bars, which indicate standard deviation, are obscured by the symbols.

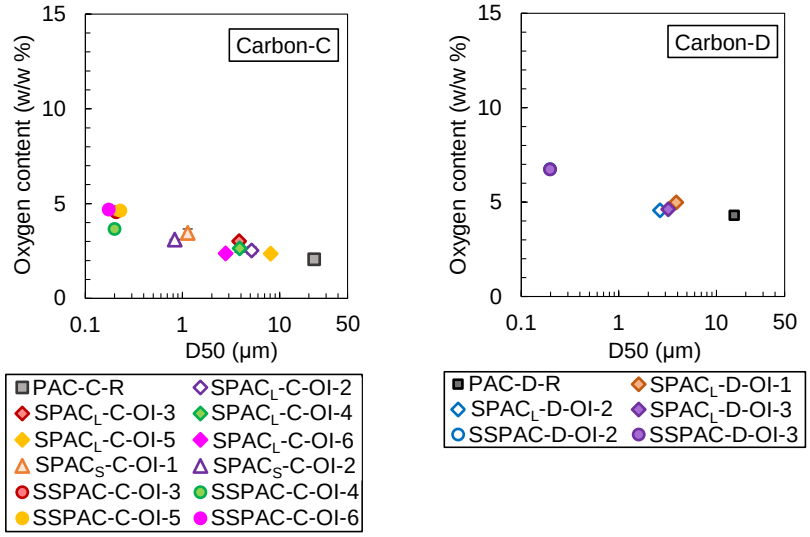

Fig. 5 – Plots of oxygen contents of Carbons C and D produced by oxidation-inhibiting milling versus AC particle size. Squares indicate PAC, diamonds indicate $SPAC_L$, triangles indicate $SPAC_S$, and circles indicate SSPAC. Error bars, which indicate standard deviation, are obscured by the symbols.

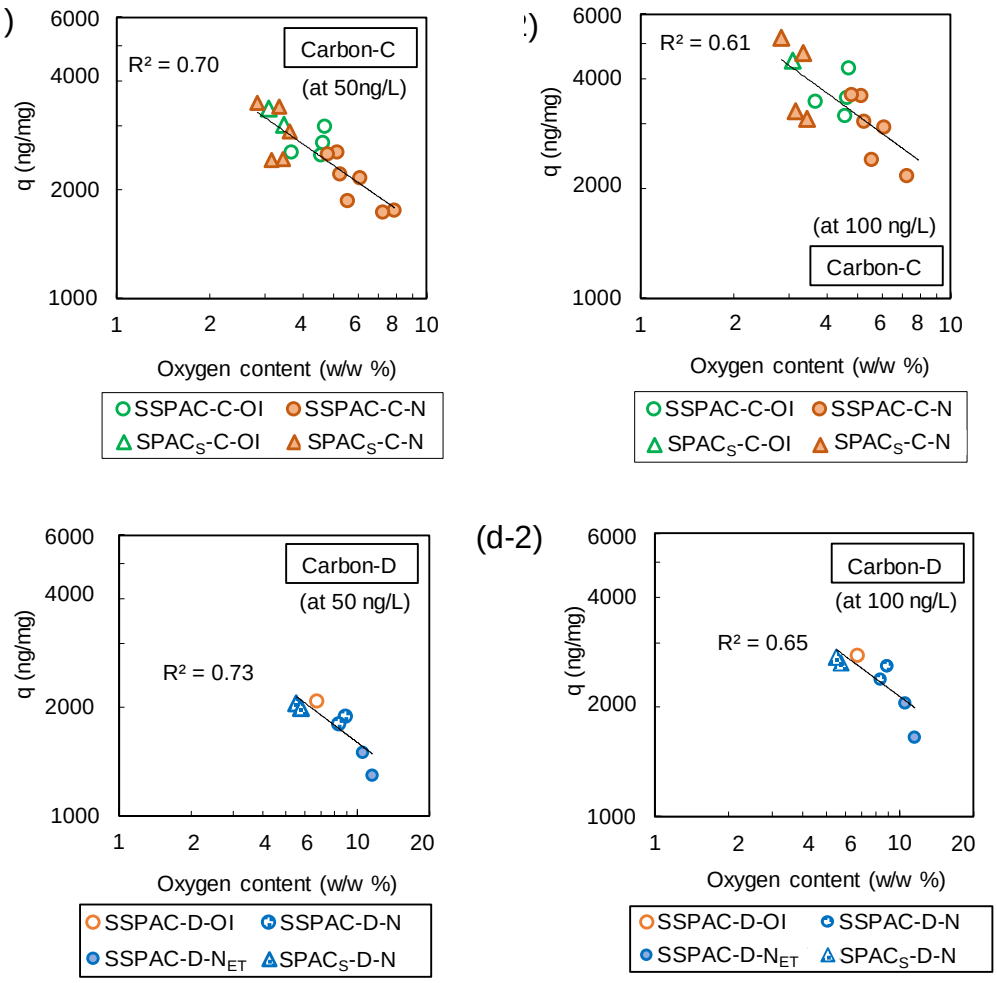

Fig. 6 – Correlation between MIB adsorption capacity and oxygen content. Triangles indicate $SPAC_S$, and circles indicate SSPAC.

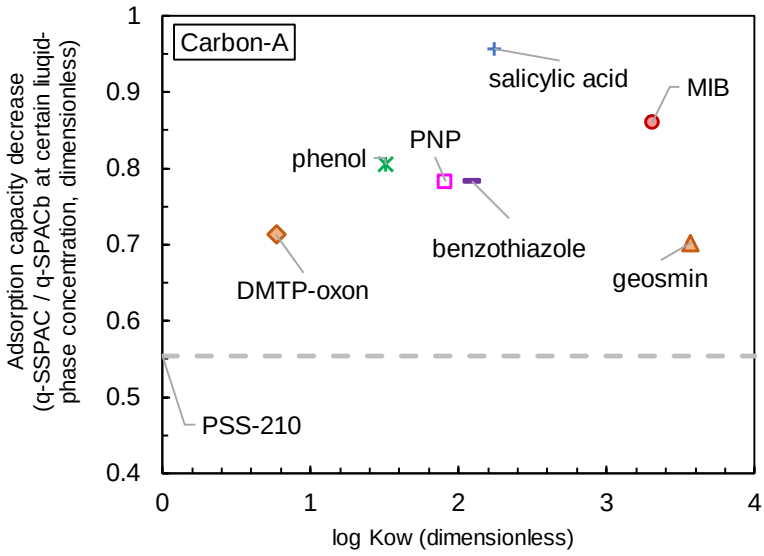

Fig. 7 – Plot of ratios of SPAC$_S$ and SSPAC adsorption capacities versus adsorbate log Kow.

The adsorption capacities were quantified in terms of the solid-phase adsorbate concentrations at equilibrium liquid-phase concentrations: MIB and geosmin, 50 ng/L; DMTP-oxon, 5 µg/L; benzothiazole, phenol, *para*-nitrophenol (PNP), and salicylic acid, 0.5 mg/L; PSS-210, 2 mg/L. The ratio for PSS-210 is indicated by a dashed line because the log Kow is unavailable.

Supplementary Information

Effects of Decreasing Activated Carbon Particle Diameter from 30 μm to 140 nm on Equilibrium Adsorption Capacity

Long Pan[a], Yuki Nishimura[a], Hideki Takaesu[a], Yoshihiko Matsui[b]*, Taku Matsushita[b], Nobutaka Shirasaki[b]

[a] Graduate School of Engineering, Hokkaido University, N13W8, Sapporo 060-8628, Japan

[b] Faculty of Engineering, Hokkaido University, N13W8, Sapporo 060-8628, Japan

* Corresponding author. Tel./fax: +81-11-706-7280

E-mail address: matsui@eng.hokudai.ac.jp

Table S1 – Characteristics of normally milled PACs, SPACs, and SSPACs.

Designation	Median diameter D_{50} (µm)	Mill	Source carbon	Median diameter D_{50} (µm)
$SPAC_L$-A-N	not measured	Ball mill	PAC-A	12.0
$SPAC_S$-A-N	1.47	Bead mill	$SPAC_L$-A-N	not measured
SSPAC-A-N	0.198		$SPAC_S$-A-N	1.47
$SPAC_L$-B-N	3.85	Ball mill	PAC-B	27.5
$SPAC_S$-B-N	1.21	Bead mill	$SPAC_L$-B-N	3.85
SSPAC-B-N	0.194		$SPAC_S$-B-N	1.21
$SPAC_L$-C-N-1	not measured	Ball mill	PAC-C	23.1
$SPAC_L$-C-N-2	4.00			
$SPAC_L$-C-N-3	3.87			
$SPAC_L$-C-N-4	4.04			
$SPAC_L$-C-N-5	3.79			
$SPAC_S$-C-N-1	1.12	Bead mill	$SPAC_L$-C-N-1	not measured
$SPAC_S$-C-N-2	0.949		$SPAC_L$-C-N-2	4.00
$SPAC_S$-C-N-3	1.64		$SPAC_L$-C-N-3	3.87
$SPAC_S$-C-N-4	1.30		$SPAC_L$-C-N-4	4.04
$SPAC_S$-C-N-5	not measured		$SPAC_L$-C-N-5	3.79
$SPAC_S$-C-N-6	1.45		$SPAC_L$-C-N-6	4.44
SSPAC-C-N-1	0.176		$SPAC_L$-C-N-1	not measured
SSPAC-C-N-2	0.137		$SPAC_L$-C-N-2	4.00
SSPAC-C-N-3	0.179		$SPAC_L$-C-N-3	3.87
SSPAC-C-N-4	0.177		$SPAC_L$-C-N-4	4.04
SSPAC-C-N-5	0.177		$SPAC_L$-C-N-5	3.79
$SPAC_L$-D-N-1	3.03	Ball mill	PAC-D	15.5
$SPAC_L$-D-N-2	3.57			
$SPAC_L$-D-N-3	3.00			
$SPAC_S$-D-N-1	0.927	Bead mill	$SPAC_L$-D-N-1	3.03
$SPAC_S$-D-N-2	0.915		$SPAC_L$-D-N-2	3.57
$SPAC_S$-D-N-3	0.927		$SPAC_S$-D-N-3	3.00
SSPAC-D-N-1	0.169		$SPAC_L$-D-N-1	3.03
SSPAC-D-N-2	0.164		$SPAC_L$-D-N-2	3.57
SSPAC-D-N-3	0.169		$SPAC_S$-D-N-3	3.00
SSPAC-D-N_{ET}-3	0.168		$SPAC_S$-D-N-3	3.00
SSPAC-D-N_{ET}-4	0.170		$SPAC_S$-D-N-3	3.00
$SPAC_L$-E-N	3.90	Ball mill	PAC-E	19.5
$SPAC_S$-E-N	1.19	Bead mill	$SPAC_L$-E-N	3.90
SSPAC-E-N	0.177		$SPAC_L$-E-N	3.90

Table S2 – Characteristics of PACs, SPACs, and SSPACs produced by rinsing with pure water (R) and by oxidation-inhibiting milling (OI).

Designation	Median diameter D_{50} (µm)	Milling system	Detail Production method			Source carbon
			Rotational speed (rpm)	Bead/ball diameter (mm)	Slurry volume (mL)	
PAC-B-R	21.7	no				PAC-B
$SPAC_L$-B-OI	not measured	Ball mill – N_2 filled	45	5 & 10	100	PAC-B-R
$SPAC_S$-B-OI	0.794	Bead mill – N_2 purging	2590	0.3	400 - 500	$SPAC_L$-B-OI
SSPAC-B-OI	0.230			0.1		$SPAC_L$-B-OI
PAC-C-R	22.7	no				PAC-C
$SPAC_L$-C-OI-1	not measured	Ball mill – N_2 filled	45	5 & 10	100	PAC-C-R
$SPAC_L$-C-OI-2	5.15					
$SPAC_L$-C-OI-3	3.82					
$SPAC_L$-C-OI-4	3.88					
$SPAC_L$-C-OI-5	8.11					
$SPAC_L$-C-OI-6	2.78					
$SPAC_S$-C-OI-1	1.13	Bead mill – N_2 purging	2590	0.3	400 - 500	$SPAC_L$-C-OI-1
$SPAC_S$-C-OI-2	0.831					$SPAC_L$-C-OI-2
SSPAC-C-OI-3	0.213			0.1		$SPAC_L$-C-OI-3
SSPAC-C-OI-4	0.200			0.3		$SPAC_L$-C-OI-4
SSPAC-C-OI-5	0.229					$SPAC_L$-C-OI-5
SSPAC-C-OI-6	0.174			0.1		$SPAC_L$-C-OI-6
PAC-D-R	15.3	no				PAC-D
$SPAC_L$-D-OI-1	3.87	Ball mill – N_2 filled	45	5 & 10	100	PAC-D-R
$SPAC_L$-D-OI-2	2.65					
$SPAC_L$-D-OI-3	3.21					
SSPAC-D-OI-2	0.197	Bead mill – N_2 purging	2590	0.1	400 - 500	$SPAC_L$-D-OI-2
SSPAC-D-OI-3	0.197					$SPAC_L$-D-OI-3

Table S3 – Composition of the working solution.

Ion	Na^+	K^+	Mg^{2+}	Ca^{2+}	Cl^-	NO^{3-}	SO_4^{2-}	Alkalinity
Concentration (mg/L)	19	3.1	24	18	31	6.9	14	50

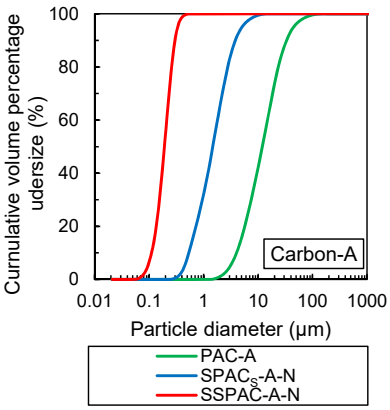
Cumulative volume percentage udersize (%)
100
80
60
40
20
0
0.01
0.1
1
10
100
1000
Particle diameter (μm)
Carbon-A
PAC-A
SPAC$_S$-A-N
SSPAC-A-N

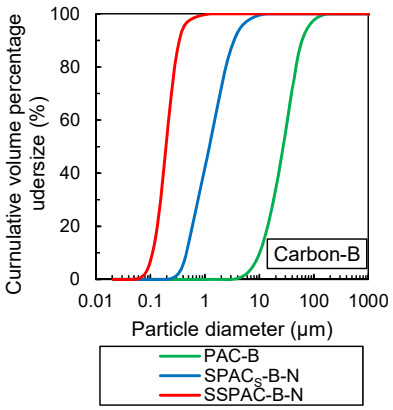
Cumulative volume percentage udersize (%)
100
80
60
40
20
0
0.01
0.1
1
10
100
1000
Particle diameter (μm)
Carbon-B
PAC-B
SPAC$_S$-B-N
SSPAC-B-N

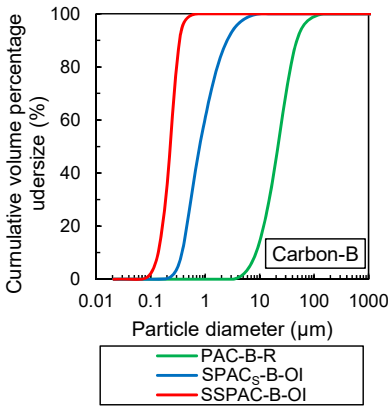
Cumulative volume percentage udersize (%)
100
80
60
40
20
0
0.01
0.1
1
10
100
1000
Particle diameter (μm)
Carbon-B
PAC-B-R
SPAC$_S$-B-OI
SSPAC-B-OI

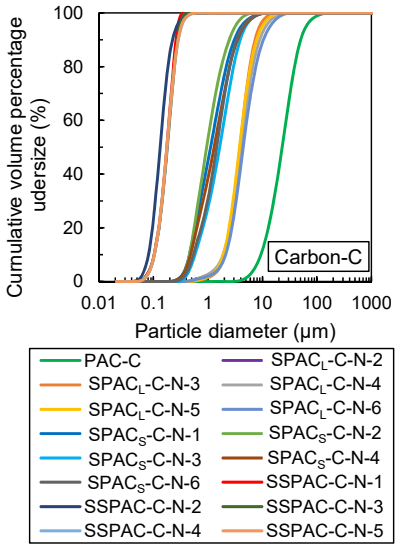
Cumulative volume percentage udersize (%)
100
80
60
40
20
0
0.01
0.1
1
10
100
1000
Particle diameter (μm)
Carbon-C
PAC-C
SPAC$_L$-C-N-2
SPAC$_L$-C-N-3
SPAC$_L$-C-N-4
SPAC$_L$-C-N-5
SPAC$_L$-C-N-6
SPAC$_S$-C-N-1
SPAC$_S$-C-N-2
SPAC$_S$-C-N-3
SPAC$_S$-C-N-4
SPAC$_S$-C-N-6
SSPAC-C-N-1
SSPAC-C-N-2
SSPAC-C-N-3
SSPAC-C-N-4
SSPAC-C-N-5

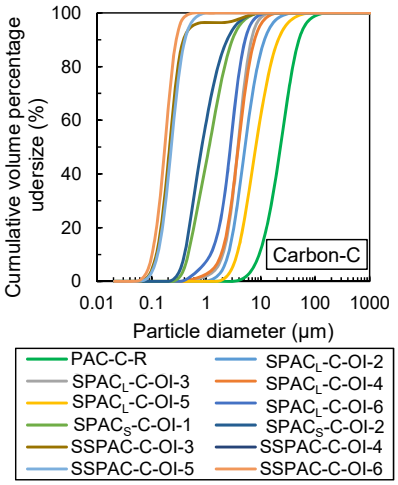
Cumulative volume percentage udersize (%)
100
80
60
40
20
0
0.01
0.1
1
10
100
1000
Particle diameter (μm)
Carbon-C
PAC-C-R
SPAC$_L$-C-OI-2
SPAC$_L$-C-OI-3
SPAC$_L$-C-OI-4
SPAC$_L$-C-OI-5
SPAC$_L$-C-OI-6
SPAC$_S$-C-OI-1
SPAC$_S$-C-OI-2
SSPAC-C-OI-3
SSPAC-C-OI-4
SSPAC-C-OI-5
SSPAC-C-OI-6

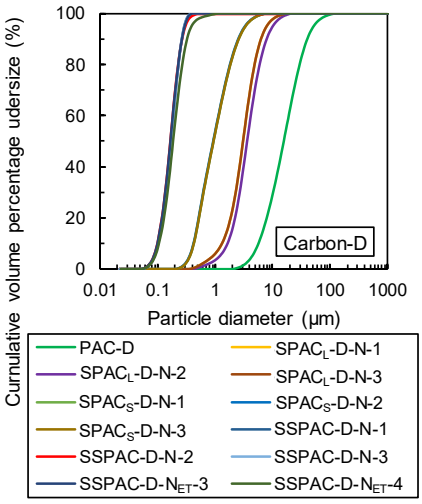
Cumulative volume percentage udersize (%)
100
80
60
40
20
0
0.01
0.1
1
10
100
1000
Particle diameter (μm)
Carbon-D
PAC-D
SPAC$_L$-D-N-1
SPAC$_L$-D-N-2
SPAC$_L$-D-N-3
SPAC$_S$-D-N-1
SPAC$_S$-D-N-2
SPAC$_S$-D-N-3
SSPAC-D-N-1
SSPAC-D-N-2
SSPAC-D-N-3
SSPAC-D-N$_{ET}$-3
SSPAC-D-N$_{ET}$-4

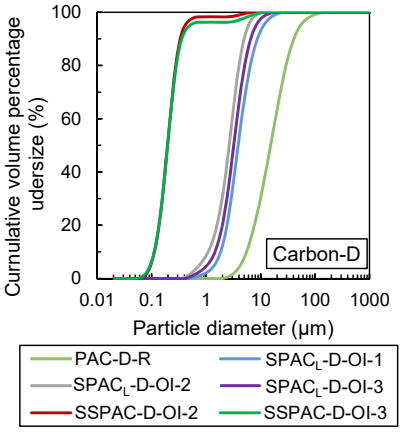
Cumulative volume percentage udersize (%)
100
80
60
40
20
0
0.01
0.1
1
10
100
1000
Particle diameter (μm)
Carbon-D
PAC-D-R
SPAC$_L$-D-OI-1
SPAC$_L$-D-OI-2
SPAC$_L$-D-OI-3
SSPAC-D-OI-2
SSPAC-D-OI-3

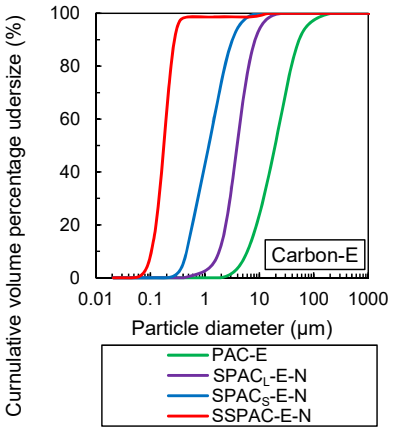

Fig. S1 – Particle size distributions of PACs, SPACs, and SSPACs.

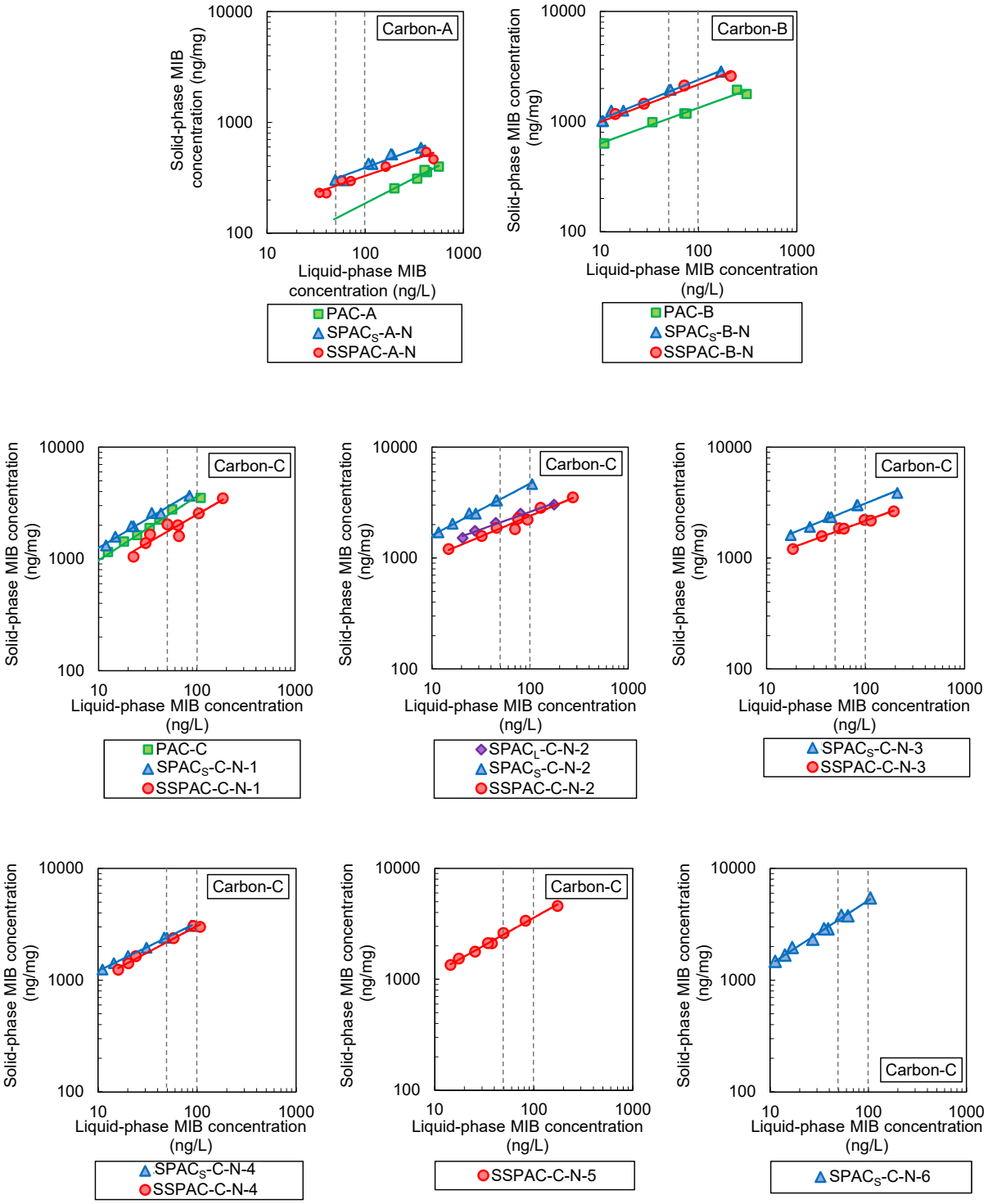
Carbon-A
Solid-phase MIB concentration (ng/mg)
10000
1000
100
10
100
1000
Liquid-phase MIB concentration (ng/L)
PAC-A
SPAC$_S$-A-N
SSPAC-A-N
Carbon-B
Solid-phase MIB concentration (ng/mg)
Liquid-phase MIB concentration (ng/L)
PAC-B
SPAC$_S$-B-N
SSPAC-B-N
Carbon-C
Solid-phase MIB concentration (ng/mg)
Liquid-phase MIB concentration (ng/L)
PAC-C
SPAC$_S$-C-N-1
SSPAC-C-N-1
SPAC$_L$-C-N-2
SPAC$_S$-C-N-2
SSPAC-C-N-2
SPAC$_S$-C-N-3
SSPAC-C-N-3
SPAC$_S$-C-N-4
SSPAC-C-N-4
SSPAC-C-N-5
SPAC$_S$-C-N-6

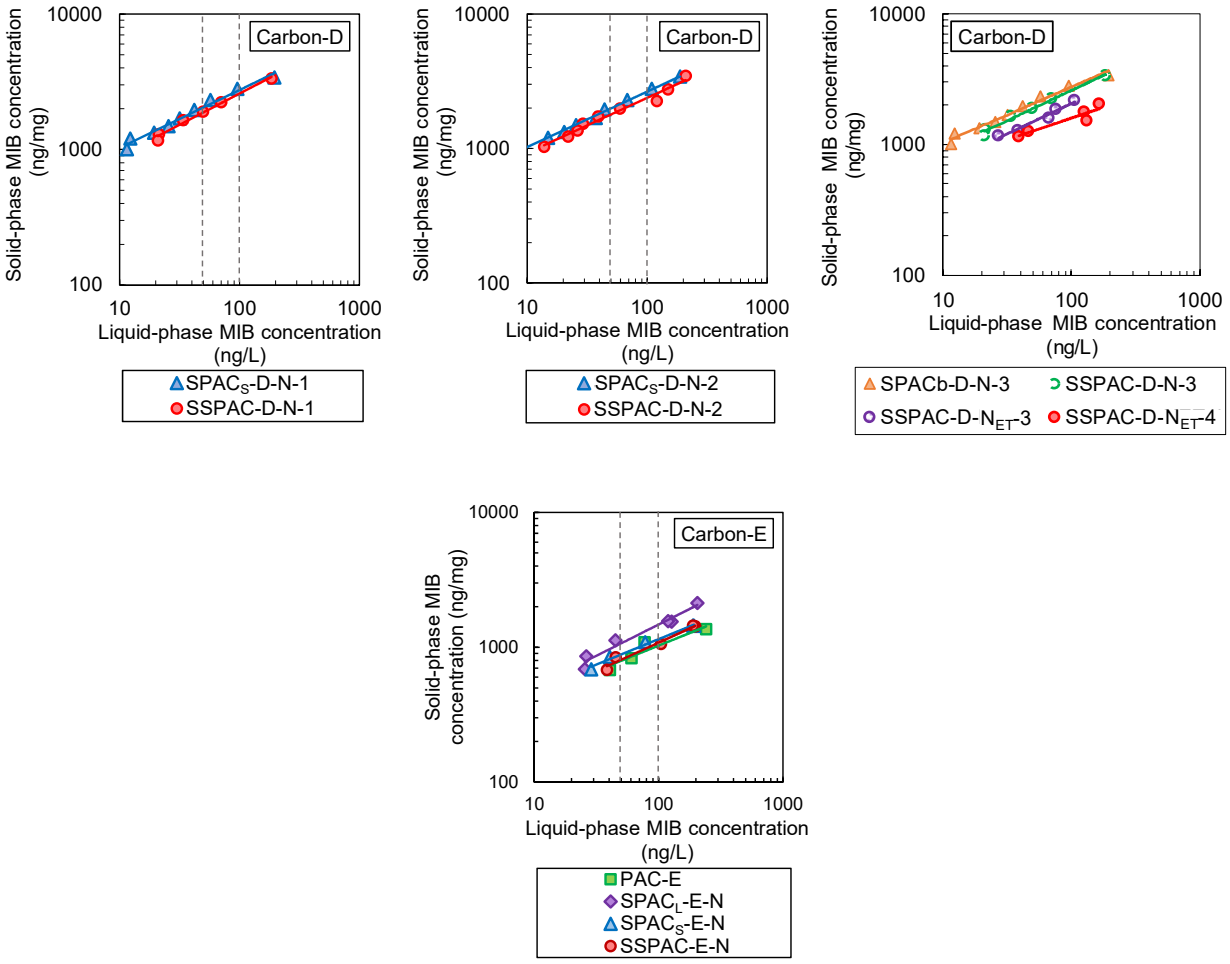

Fig. S2 – MIB adsorption isotherms for Carbons A–E. Squares indicate PAC, diamonds indicate $SPAC_L$, triangles indicate $SPAC_S$, and circles indicate SSPAC.

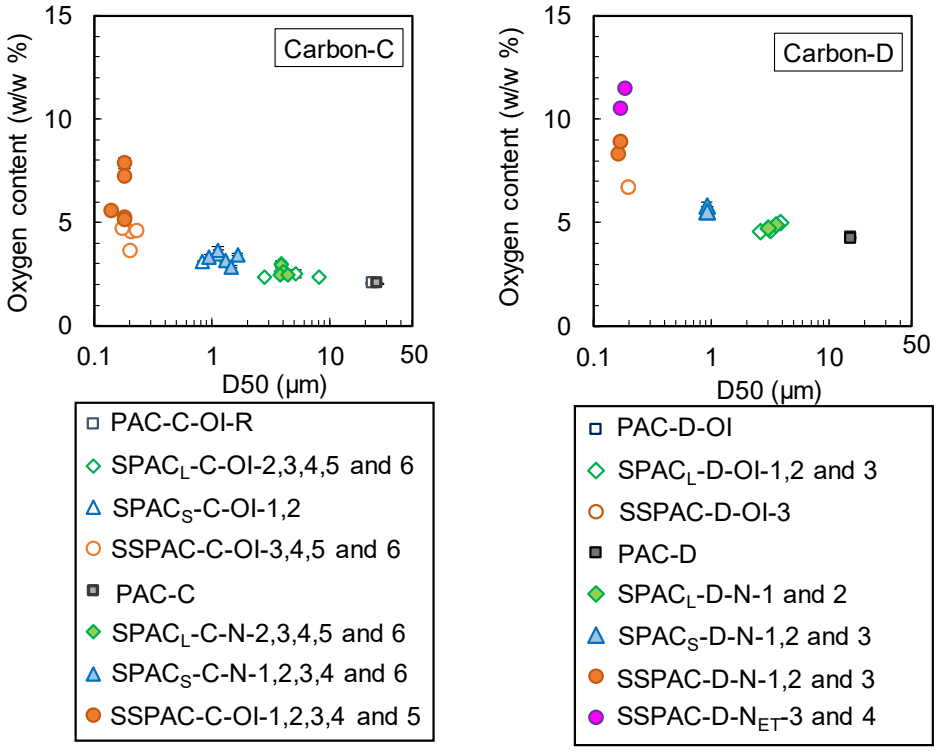

Fig. S3 –Plots of oxygen contents of Carbons C and D produced by normal and oxidation-inhibiting millings versus AC particle size. Squares indicate PAC, diamonds indicate SPACL, triangles indicate SPACS, and circles indicate SSPAC. Closed plots indicate carbons produced by normal milling and open plots indicate those by oxidation-inhibiting milling. Error bars, which indicate standard deviation, are obscured by the symbols.

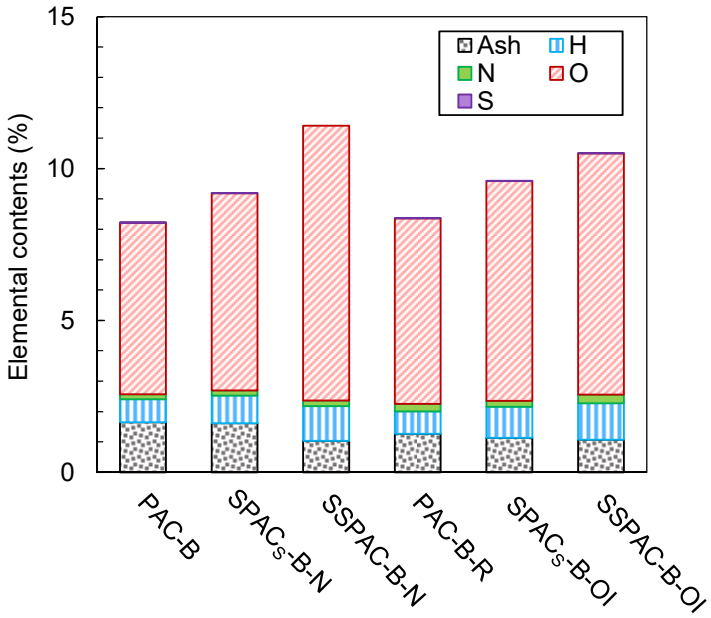

Fig. S4 – Hydrogen, nitrogen, sulfur, oxygen, and ash contents of Carbons-B produced by normal milling and oxygen-inhibiting milling.

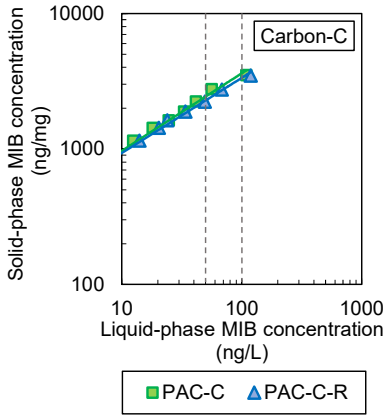

Fig. S5 – MIB adsorption isotherms of PAC-C-N and PAC-C-R (produced by rinsing PAC-C-N with pure water).

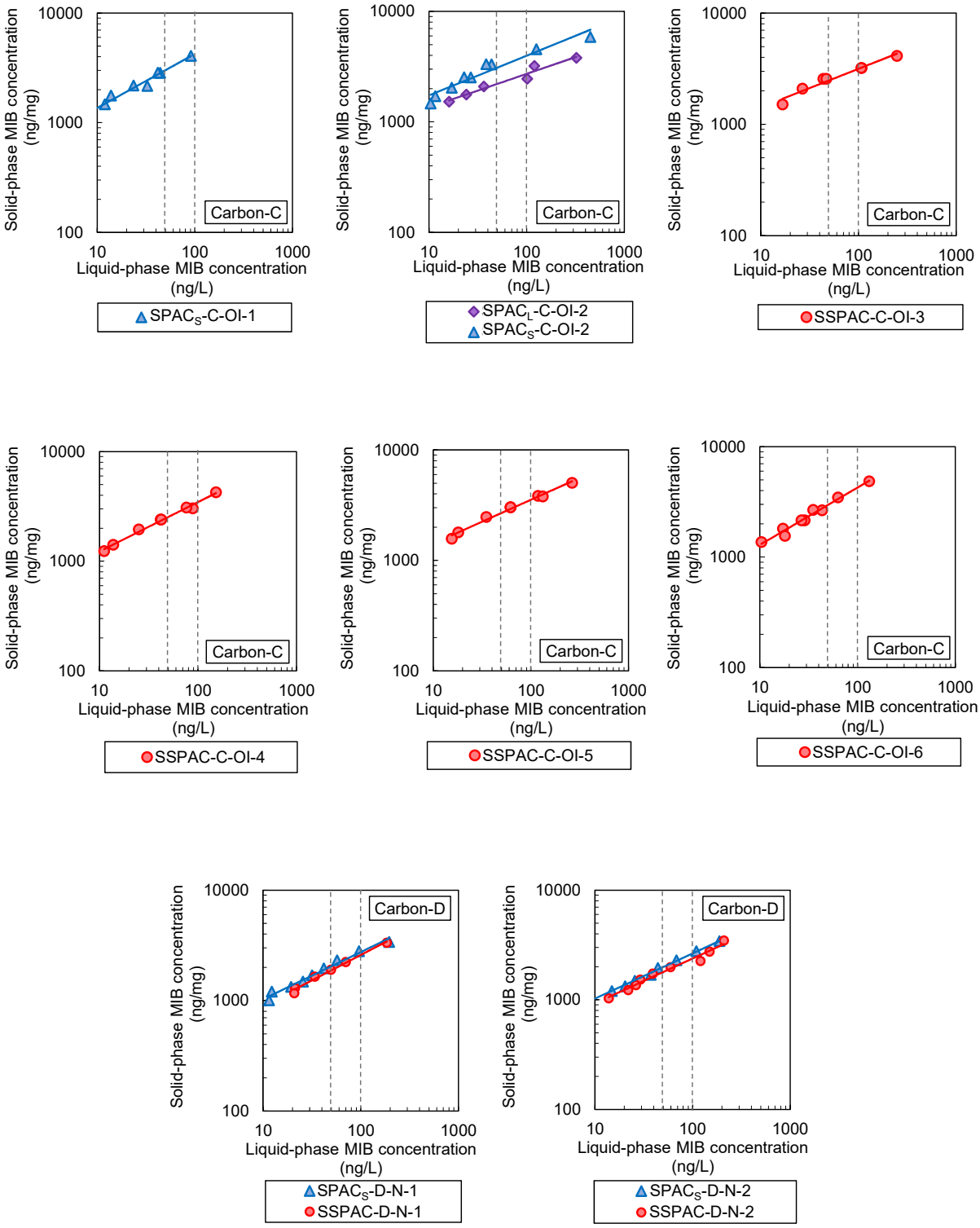

Fig. S6 – MIB adsorption isotherms for $SPAC_L$, $SPAC_S$, and SSPAC prepared from Carbons C and D by oxidation-inhibiting milling. Diamonds indicate $SPAC_L$, triangles indicate $SPAC_S$, and circles indicate SSPAC.

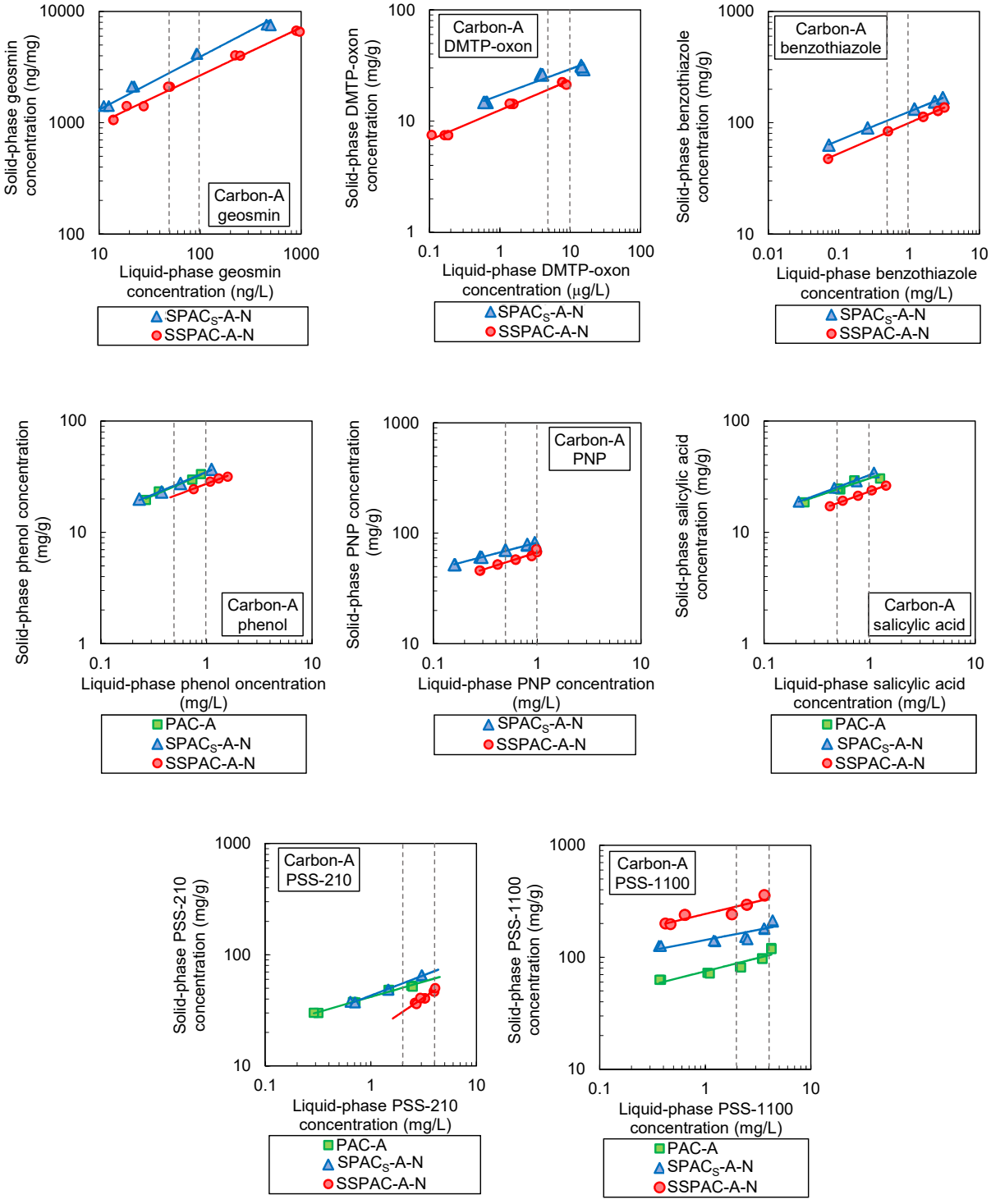
Solid-phase geosmin concentration (ng/mg)
10000
1000
100
10
100
1000
Liquid-phase geosmin concentration (ng/L)
Carbon-A geosmin
SPACS-A-N
SSPAC-A-N
Solid-phase DMTP-oxon concentration (mg/g)
100
10
1
0.1
1
10
100
Liquid-phase DMTP-oxon concentration (μg/L)
Carbon-A DMTP-oxon
SPACS-A-N
SSPAC-A-N
Solid-phase benzothiazole concentration (mg/g)
1000
100
10
0.01
0.1
1
10
Liquid-phase benzothiazole concentration (mg/L)
Carbon-A benzothiazole
SPACS-A-N
SSPAC-A-N
Solid-phase phenol concentration (mg/g)
100
10
1
0.1
1
10
Liquid-phase phenol oncentration (mg/L)
Carbon-A phenol
PAC-A
SPACS-A-N
SSPAC-A-N
Solid-phase PNP concentration (mg/g)
1000
100
10
0.1
1
10
Liquid-phase PNP concentration (mg/L)
Carbon-A PNP
SPACS-A-N
SSPAC-A-N
Solid-phase salicylic acid concentration (mg/g)
100
10
1
0.1
1
10
Liquid-phase salicylic acid concentration (mg/L)
Carbon-A salicylic acid
PAC-A
SPACS-A-N
SSPAC-A-N
Solid-phase PSS-210 concentration (mg/g)
1000
100
10
0.1
1
10
Liquid-phase PSS-210 concentration (mg/L)
Carbon-A PSS-210
PAC-A
SPACS-A-N
SSPAC-A-N
Solid-phase PSS-1100 concentration (mg/g)
1000
100
10
0.1
1
10
Liquid-phase PSS-1100 concentration (mg/L)
Carbon-A PSS-1100
PAC-A
SPACS-A-N
SSPAC-A-N

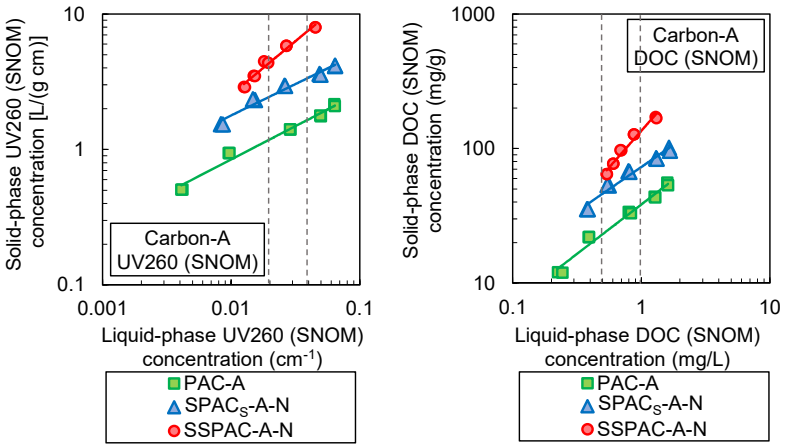

Fig. S7 – Isotherms for adsorption of 9 adsorbates on Carbons A. Squares indicate PAC, triangles indicate $SPAC_S$, and circles indicate SSPAC.

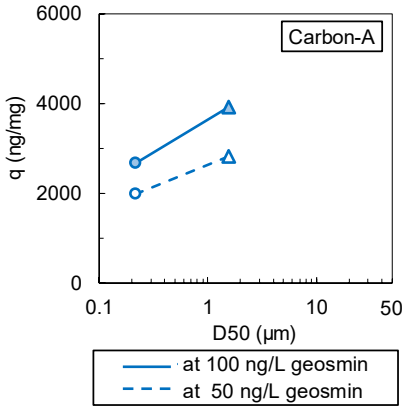
Carbon-A
q (ng/mg)
6000
4000
2000
0
0.1
1
10
50
D50 (μm)
at 100 ng/L geosmin
at 50 ng/L geosmin

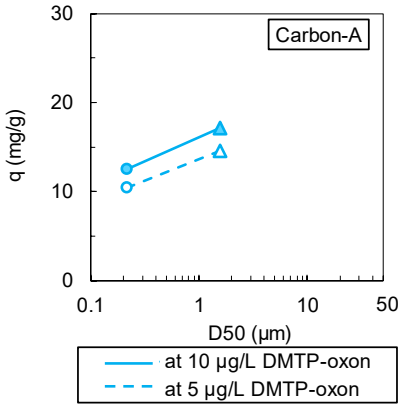
Carbon-A
q (mg/g)
30
20
10
0
0.1
1
10
50
D50 (μm)
at 10 μg/L DMTP-oxon
at 5 μg/L DMTP-oxon

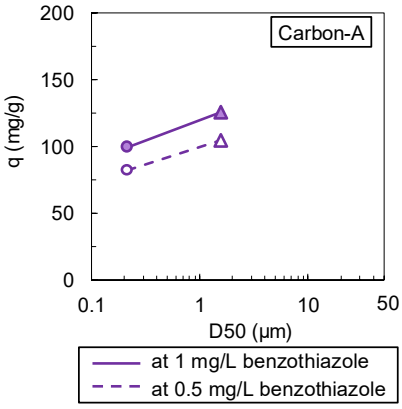
Carbon-A
q (mg/g)
200
150
100
50
0
0.1
1
10
50
D50 (μm)
at 1 mg/L benzothiazole
at 0.5 mg/L benzothiazole

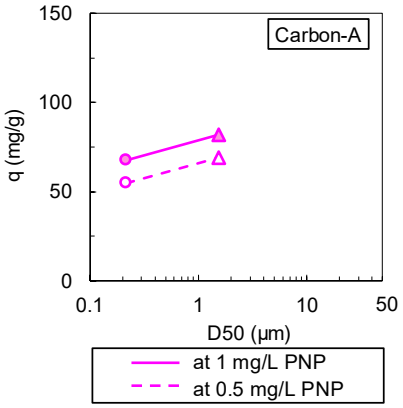
Carbon-A
q (mg/g)
150
100
50
0
0.1
1
10
50
D50 (μm)
at 1 mg/L PNP
at 0.5 mg/L PNP

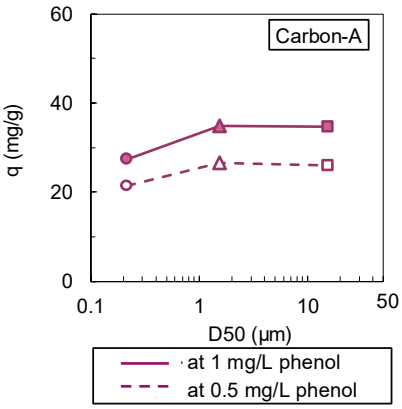
Carbon-A
q (mg/g)
60
40
20
0
0.1
1
10
50
D50 (μm)
at 1 mg/L phenol
at 0.5 mg/L phenol

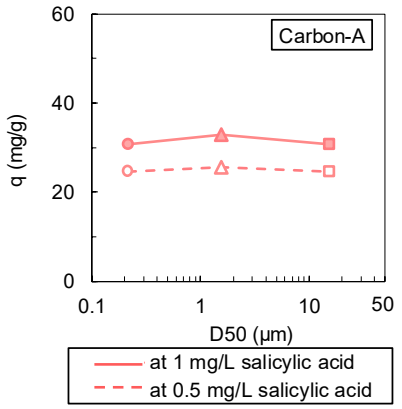
Carbon-A
q (mg/g)
60
40
20
0
0.1
1
10
50
D50 (μm)
at 1 mg/L salicylic acid
at 0.5 mg/L salicylic acid

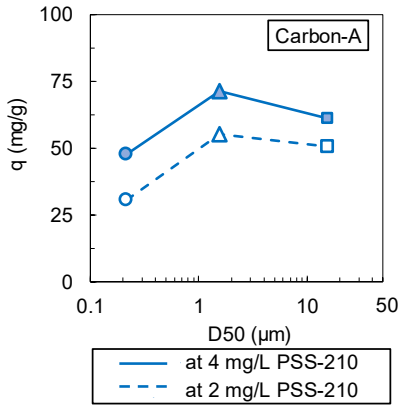
Carbon-A
q (mg/g)
100
75
50
25
0
0.1
1
10
50
D50 (μm)
at 4 mg/L PSS-210
at 2 mg/L PSS-210

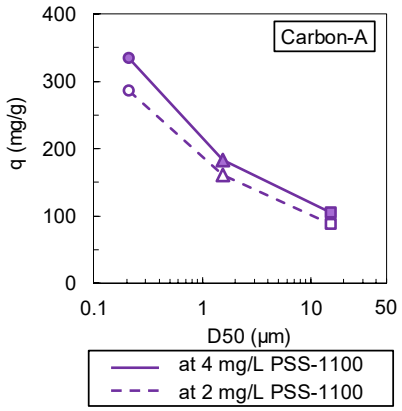
Carbon-A
q (mg/g)
400
300
200
100
0
0.1
1
10
50
D50 (μm)
at 4 mg/L PSS-1100
at 2 mg/L PSS-1100

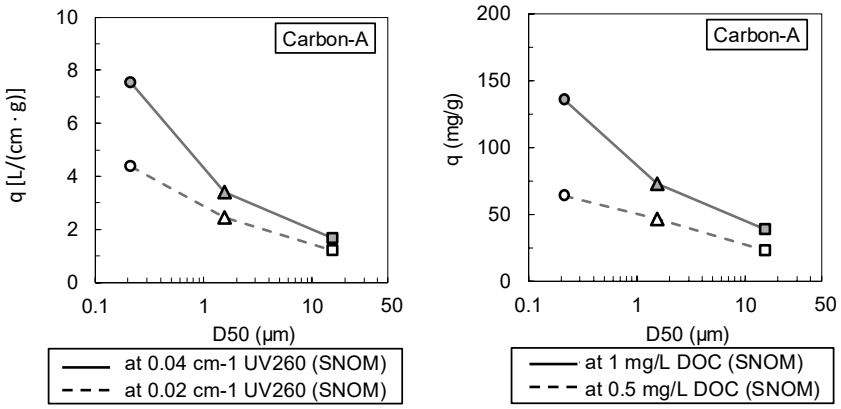

Fig. S8 – Plots of equilibrium adsorption capacity versus particle size (Carbon A) for 9 adsorbates. Squares indicate PAC, triangles indicate $SPAC_S$, and circles indicate SSPAC.

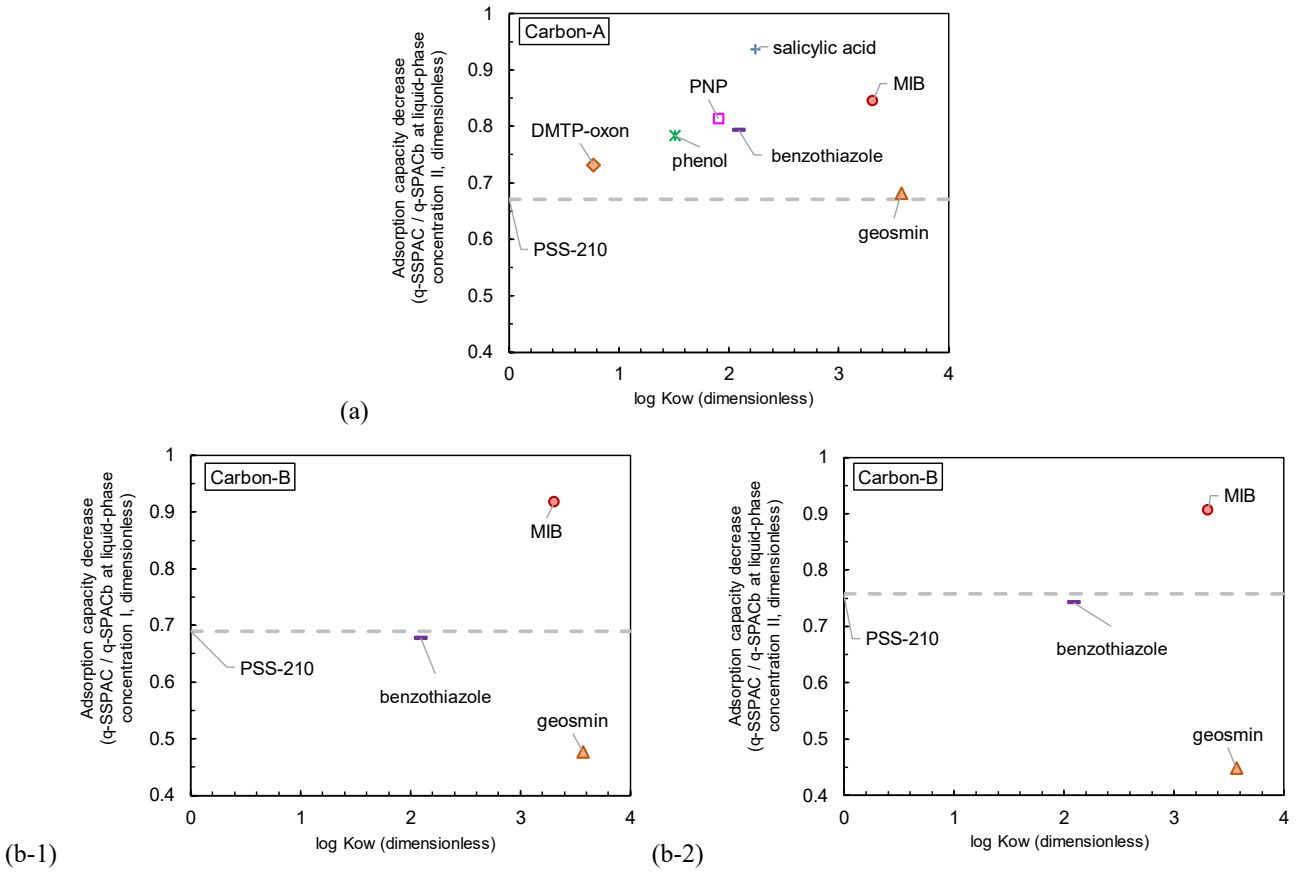

Fig. S9 – Plots of ratios of SPACs and SSPAC adsorption capacities versus adsorbate log Kow. Adsorbate concentrations I and II (panels b-1 and b-2, respectively): MIB and geosmin, 50 and 100 ng/L; DMTP-oxon, 5 and 10 µg/L; benzothiazole, phenol, *para*-nitrophenol (PNP), and salicylic acid, 0.5 and 1 mg/L; PSS-210, 2 and 4 mg/L. The ratios for PSS-210 are indicated by the dashed lines because the log Kow value is unavailable.